Nodal structure of unconventional superconductors probed by angle resolved thermal transport measurements

2006 J. Phys.: Condens. Matter 18 R705

(http://iopscience.iop.org/0953-8984/18/44/R01)

INSTITUTE OF PHYSICS PUBLISHING JOURNAL OF PHYSICS: CONDENSED MATTER

J. Phys.: Condens. Matter **18** (2006) R705–R752 doi:10.1088/0953-8984/18/44/R01

TOPICAL REVIEW

Nodal structure of unconventional superconductors probed by angle resolved thermal transport measurements

Y Matsuda[1,2], K Izawa[2,3] and I Vekhter[4]

[1] Department of Physics, Kyoto University, Kyoto 606-8502, Japan
[2] Institute for Solid State Physics, University of Tokyo, Kashiwanoha, Kashiwa, Chiba 277-8581, Japan
[3] DRFMC/SPSMS/LCP, CEA-Grenoble, 17 rue des Martyrs 38054, Grenoble cedex 9, France
[4] Department of Physics and Astronomy, Louisiana State University, Baton Rouge, LA 70803, USA

E-mail: matsuda@scphys.kyoto-u.ac.jp

Received 24 July 2006, in final form 20 September 2006
Published 20 October 2006
Online at stacks.iop.org/JPhysCM/18/R705

Abstract

Over the past two decades, unconventional superconductivity with gap symmetry other than s wave has been found in several classes of materials, including heavy fermion, high T_c, and organic superconductors. Unconventional superconductivity is characterized by anisotropic superconducting gap functions, which may have zeros (nodes) along certain directions in the Brillouin zone. The nodal structure is closely related to the pairing interaction, and it is widely believed that the presence of nodes is a signature of magnetic or some other exotic, rather than conventional phonon mediated, pairing mechanism. Therefore experimental determination of the gap function is of fundamental importance. However, the detailed gap structure, especially the direction of the nodes, is an unresolved issue for most unconventional superconductors. Recently it has been demonstrated that thermal conductivity and specific heat measurements under a magnetic field rotated relative to the crystal axes provide a powerful method for determining the shape of the gap and the nodal directions in the bulk. Here we review the theoretical underpinnings of the method and the results for the nodal structure of several unconventional superconductors, including borocarbide YNi_2B_2C, heavy fermions UPd_2Al_3, $CeCoIn_5$, and $PrOs_4Sb_{12}$, organic superconductor κ-(BEDT-TTF)$_2$Cu(NCS)$_2$, and ruthenate Sr_2RuO_4, determined through angular variation of the thermal conductivity and heat capacity.

Contents

1. Introduction

The superconducting transition is a second order phase transition associated with a spontaneous symmetry breaking. Consequently the order parameter that appears below the transition temperature, T_c, characterizes the lowering of the symmetry in the low temperature ordered phase compared to the metallic state. The order parameter is also related to the gap in the single particle excitation spectrum, and hence its symmetry is reflected in the elementary excitations in the superconducting phase. These, in turn, determine the observed transport and thermodynamic properties [1, 2].

At the microscopic level, the symmetry of the order parameter is intimately related to the pairing interaction. Therefore the identification of this symmetry is of central importance in the study of the superconductivity, especially in novel correlated electron materials. This review describes recent progress and the current status of the efforts to use transport properties as a reliable tool for the determination of the gap symmetry in unconventional superconductors in the bulk.

In all superconductors the gauge symmetry is broken below the transition temperature. At the same time, in most materials, the energy gap has the full spatial symmetry of the underlying crystal lattice. In the simplest cases, this corresponds to a gap isotropic in the momentum space, i.e. independent of the directions at the Fermi surface. These superconductors are termed conventional, or s wave. However, it is also possible that the spatial symmetry of the superconducting order parameter is *lower* than that of the lattice, and such superconductors are labelled unconventional. Section 2 presents the detailed symmetry classification of the unconventional superconductors. These materials first appeared in 1979, when the heavy fermion $CeCu_2Si_2$ was discovered [3], and by now superconductivity with non-s wave symmetry is ubiquitous. Examples of it include anisotropic gaps with zeros (nodes), odd parity superconducting condensate wavefunctions, and broken time reversal symmetry. Realization of these possibilities is proved or strongly suggested in several classes of materials, including heavy fermion [4–6], high T_c cuprates [7], ruthenate [8–10], cobaltate [11], intermetallic compounds [12], and organic superconductors [13–16].

In these systems, strong electron correlations often give rise to the Cooper pair states with a non-zero angular momentum. Unfortunately, the experimental determination of the detailed superconducting gap structure is an extremely difficult task. The phase sensitive measurements testing the sign change of the gap have only been done for the high T_c cuprates, firmly establishing (along with a number of other techniques probing the gap anisotropy) the predominant $d_{x^2-y^2}$ pairing symmetry [7].

Unconventional superconductivity often occurs in heavy fermion compounds, containing f electrons (lanthanide (4f) and actinide (5f)), especially in materials containing Ce, Pr, U and Pu atoms. At high temperature f electrons are essentially localized with well-defined magnetic moments. As the temperature is lowered, the f electrons begin to delocalize due to the hybridization with conduction electron band (s, p, d orbital), and Kondo screening. At yet lower T, the f electrons become itinerant, forming a narrow conduction band with heavy effective electron mass (up to a few hundred to a thousand times the free electron mass). Strong Coulomb repulsion within a narrow band and the magnetic interaction between remnant unscreened 4f or 5f moments leads to notable many-body effects, and, probably, to superconductivity mediated by magnetic fluctuations. These effects are believed to be especially pronounced in the vicinity of zero temperature magnetic instability (quantum critical point (QCP)). Although the superconducting gap is thought to be unconventional in most heavy fermion superconductors, its detailed momentum dependence is an unresolved issue [4–6].

Since the discovery of superconductivity in organic materials about two decades ago, superconductivity has been reported in more than 100 organic compounds. Among them, two families of compounds, quasi-1D Bechgaard salts $(TMTSF)_2X$ ($X = ClO_4$, PF_6, AsF_6, etc) and quasi-2D κ-$(BEDT\text{-}TTF)_2X$ salts (κ-$(ET)_2X$), where the ion X can, for example, be $Cu(SCN)_2$, $Cu[N(CN)_2]Br$ or I_3, are particularly prominent candidates for unconventional pairing. The pairing symmetry in both systems is still undetermined, and is one of the most intriguing problems in the field [14–16].

The unconventional superconductivity has also been reported in some of transition metal oxides other than high T_c cuprates. In particular, the superconducting gap functions in layered ruthenate Sr_2RuO_4 [9, 10] and layered cobaltate $Na_xCoO_2{\cdot}yH_2O$ [11] have attracted considerable interest. Moreover, among intermetallic compound, the gap function of borocarbide superconductors $(Y, Lu)Ni_2B_2C$ [12] has been reported to be very anisotropic, which implies that the simple electron–phonon pairing mechanism originally envisaged for these compounds is not the sole source for pairing interaction.

Evidence for anisotropic gap in a variety of systems has continued to motivate theorists to propose new models for the unconventional superconductivity, which make specific predictions for the shape of the superconducting gap in momentum space. Experimental determination of the gap symmetry is therefore of crucial importance. The transport measurements are not, *per se*, phase sensitive, and therefore cannot unequivocally determine the sign change in the gap function. They are, however, an extremely sensitive probe of the anisotropy of the gap amplitude in the momentum space, and have been extensively used in the last few years to determine the shape of the gap in many materials at the forefront of modern research. Below we give an overview of these efforts.

2. Unconventional pairing state

The general classification scheme for the superconducting order parameter is based on its behaviour under symmetry transformations. The full symmetry group $\mathcal{G}$ of the crystal contains the gauge group $U(1)$, crystal point group G, spin rotation group $SU(2)$, and time reversal symmetry group $\mathcal{T}$,

$$\mathcal{G} = U(1) \otimes G \otimes SU(2) \otimes \mathcal{T}. \tag{1}$$

The superconducting order breaks the $U(1)$ gauge symmetry below T_c, and the simplest superconductors are those in which only the $U(1)$ symmetry is broken; these are labelled conventional. Unconventional superconductors break an additional symmetry besides $U(1)$, and may include order parameters which

(i) have odd parity;
(ii) break time reversal symmetry;
(iii) break the point group symmetry of the crystal.

The superconducting order parameter is proportional to the gap function $\Delta^{\ell}_{\mathbf{s}_1,\mathbf{s}_2}(\mathbf{k})$, which, in turn, is proportional to the amplitude of the wavefunction for a Cooper pair $\Psi^{\ell}_{\mathbf{s}_1,\mathbf{s}_2}(\mathbf{k}) = \langle\psi_{\mathbf{k},\mathbf{s}_1}\psi_{-\mathbf{k},\mathbf{s}_2}\rangle$. Here $\mathbf{k}$ is the quasiparticle momentum, $\mathbf{s}_i$ is the electron spin, and ψ is the electron annihilation operator. The order parameter is called unconventional if it transforms according to a non-trivial representation of the full symmetry group. Pauli's exclusion principle requires $\Delta^{\ell}_{\mathbf{s}_1,\mathbf{s}_2}(\mathbf{k})$ to be antisymmetric under the particle interchange: $\Delta^{\ell}_{\mathbf{s}_1,\mathbf{s}_2}(\mathbf{k}) = -\Delta^{\ell}_{\mathbf{s}_2,\mathbf{s}_1}(-\mathbf{k})$. In the simplest case of weak spin–orbit interaction, the total angular momentum $\mathbf{L}$ and total spin $\mathbf{S} = \mathbf{s}_1 + \mathbf{s}_2$ are good quantum numbers, and $\Delta_{\mathbf{s}_1,\mathbf{s}_2}(\mathbf{k})$ can be written as a product of orbital and spin parts,

$$\Delta^{\ell}_{\mathbf{s}_1,\mathbf{s}_2}(\mathbf{k}) = g_{\ell}(\mathbf{k})\chi_{\mathrm{s}}(\mathbf{s}_1,\mathbf{s}_2). \tag{2}$$

The orbital part, $g_{\ell}(\mathbf{k})$ can be expanded in the spherical harmonics $Y_{\ell m}(\hat{\mathbf{k}})$, which are the eigenfunctions of the angular momentum operator with the momentum ℓ and its z-projections m,

$$g_{\ell}(\mathbf{k}) = \sum_{m=-\ell}^{\ell} a_{\ell m}(k)Y_{\ell m}(\hat{\mathbf{k}}). \tag{3}$$

Here $\hat{\mathbf{k}} = \mathbf{k}/k_{\mathrm{F}}$ denotes the direction of the Fermi surface. $g_{\ell}(\mathbf{k})$ is even for even values of ℓ and odd for odd values of ℓ, $g_{\ell}(\mathbf{k}) = (-1)^{\ell}g_{\ell}(-\mathbf{k})$, and superconductors with $\ell = 0, 1, 2, 3, 4, \ldots$ are labelled as having s, p, d, f, g, ... wave gap respectively. This classification is valid for an isotropic system. In a crystal, the spatial part of the Cooper pair wavefunction is classified according to the irreducible representations of the symmetry group of the lattice. However it is common even in this case to refer to the possible pairing states as having a particular angular momentum (rather than belonging to a representation of the group with given symmetry properties) and we use the notation here.

The spin part of the order parameter, $\chi_{\mathrm{s}}(\mathbf{s}_1,\mathbf{s}_2)$, is a product of the spinors for the two electrons in the Cooper pair. Therefore the gap function is a 2×2 matrix in spin space,

$$\mathbf{\Delta}^{\ell}_{\mathbf{S}}(\mathbf{k}) \equiv \mathbf{\Delta}^{\ell}_{\mathbf{s}_1,\mathbf{s}_2}(\mathbf{k}) = \begin{pmatrix} \Delta^{\ell}_{\uparrow\uparrow}(\mathbf{k}) & \Delta^{\ell}_{\uparrow\downarrow}(\mathbf{k}) \\ \Delta^{\ell}_{\downarrow\uparrow}(\mathbf{k}) & \Delta^{\ell}_{\downarrow\downarrow}(\mathbf{k}) \end{pmatrix}. \tag{4}$$

In the singlet state, $S = 0$, the spin part of the wavefunction is $|\uparrow\downarrow\rangle - |\downarrow\uparrow\rangle$, and therefore the gap function is simply proportional to the Pauli matrix σ_y:

$$\mathbf{\Delta}_{\mathrm{s}}(\mathbf{k}) = \Delta g_{\ell}(\mathbf{k})\mathrm{i}\sigma_y, \tag{5}$$

where ℓ is even. The energy of single particle excitations in this case is

$$E_{\mathbf{k}} = \sqrt{\xi^2_{\mathbf{k}} + \Delta^2|g(\mathbf{k})|^2}, \tag{6}$$

where $\xi_{\mathbf{k}}$ is the band energy relative to the chemical potential. For superconductors with an isotropic $\Delta(\mathbf{k})$ the excitations have a finite energy gap everywhere at the Fermi surface, while for anisotropic pairing the gap amplitude depends on the components of $g(\mathbf{k})$.

For spin triplet pairing ($S = 1$), the wavefunction has components corresponding to the three different spin projections, S^z, on the quantization axis ($|\uparrow\uparrow\rangle$, $|\uparrow\downarrow\rangle + |\downarrow\uparrow\rangle$, $|\downarrow\downarrow\rangle$). Consequently, it is common to write the order parameter as

$$\begin{aligned}\mathbf{\Delta}_t(\mathbf{k}) &= \mathrm{i}(\mathbf{d}(\mathbf{k})\boldsymbol{\sigma})\sigma_y \\ &= \begin{pmatrix} -d_x(\mathbf{k}) + \mathrm{i}d_y(\mathbf{k}) & d_z(\mathbf{k}) \\ d_z(\mathbf{k}) & d_x(\mathbf{k}) + \mathrm{i}d_y(\mathbf{k}) \end{pmatrix}. \end{aligned} \tag{7}$$

The orbital part is expressed by these $\mathbf{d}$ vectors with

$$g_1 = -d_x + \mathrm{i}d_y, \qquad g_2 = d_z, \qquad g_3 = d_x + \mathrm{i}d_y, \tag{8}$$

and the excitation energy is

$$E_{\mathbf{k}} = \sqrt{\xi_{\mathbf{k}}^2 + \Delta^2|\mathbf{d}(\mathbf{k})|^2}. \tag{9}$$

In the presence of strong spin–orbit coupling only the total angular momentum $\mathbf{J} = \mathbf{L} + \mathbf{S}$ is a good quantum number, and the classification according to physical electron spin is not possible. However, if the crystal structure has an inversion centre, Cooper pair states can still be classified according to their parity, and therefore acquire a 'pseudospin' quantum number, instead of the physical spin. This situation is commonly encountered in many heavy fermion materials.

Experimentally, the parity of the pair wavefunction $\Psi_{\mathrm{pair}}(\mathbf{k})$ can be determined by the Knight shift of the nuclear magnetic resonance (NMR) frequency [2, 17], muon spin rotation (μSR), and, less directly, by the magnitude of the upper critical field H_{c2}. The Knight shift is linear in the electron spin susceptibility χ_s, and is therefore a direct measure of the spin polarization in the superconducting state. In a spin singlet superconductor, as Cooper pairs are formed, the spin contribution to the Knight shift falls rapidly on cooling through the transition. In contrast, in a triplet superconductor the spin orientation of the Cooper pairs is determined by the $\mathbf{d}$ vector in equation (7). If the direction $\mathbf{d}$ is fixed by the spin–orbit interaction, the Knight shift is anisotropic in the superconducting state. When the magnetic field is applied along $\mathbf{d}$ ($\mathbf{H} \parallel \mathbf{d}$), the Cooper pair spin is perpendicular to $\mathbf{H}$ and hence does not contribute to the susceptibility. Then the Knight shift decreases rapidly below T_c, as in spin singlet superconductors. On the other hand, when the applied field $\mathbf{H} \perp \mathbf{d}$, the x and y components of the $\mathbf{d}$ vector, $d_x(\mathbf{k}) + \mathrm{i}d_y(\mathbf{k})$, are non-zero, and the contribution to the susceptibility of the Cooper pairs is identical to that of the constituent electrons, $\chi_\parallel = \chi_n$, where n labels the normal state above the transition temperature. Therefore the Knight shift remains unchanged below T_c.

Applied magnetic field destroys superconductivity through both the orbital dephasing and Zeeman splitting of the single electron energy levels. In type II superconductors the former effect leads to the emergence of the vortex state, when the magnetic field penetrates into the sample, forming the regular array of the vortex tubes parallel to the field. Vortices have cores of the size of the superconducting coherence length, ξ, where superconductivity is destroyed. Each vortex carries a flux quantum $\Phi_0 = \pi\hbar c/e = 2 \times 10^{-7}$ G cm^2, and therefore in the external field, H, the area per vortex, A, is determined from $AH = \Phi_0$. At the orbital upper critical field the vortex cores overlap destroying bulk superconductivity, and hence a simple estimate gives $H_{c2}^O = \Phi_0/2\pi\xi^2$. On the other hand, in singlet superconductors, an additional pair breaking effect of the field is due to polarization of the normal state electrons. The upper critical field determined by this Pauli limiting effect is estimated to be $H_{c2}^{\mathrm{P}} = \Delta/\sqrt{2}\,\mu_{\mathrm{B}}$, where μ_{B} is the Bohr magneton, and Δ is superconducting gap. The Pauli limiting is absent in spin triplet superconductors. Therefore, finding H_{c2} which is higher than H_{c2}^{P} may indicate spin triplet pairing.

Up to now, a possible odd parity superconducting state has been suggested in heavy fermion UPt_3 [18], UNi_2Al_3 [19], URu_2Si_2 [20], UBe_{13} [21], $PrOs_4Sb_{12}$ [22], organic

$(TMTSF)_2PF_6$ [23], and transition metal oxides, Sr_2RuO_4 [24], $Sr_2Ca_{12}Cu_{24}O_{41}$ [25] and $Na_xCoO_2{\cdot}yH_2O$ [26, 27]. It is most probably realized in the ferromagnetic superconductors UGe_2 [28], URhGe [29] and UIr [30]. However, one needs to bear in mind that the odd parity in some of these materials is still controversial. In fact, analysis of the NMR spectrum in the vortex state, from which we determine the Knight shift, is not settled. Moreover the NMR experiment measures the surface area with the length scale of penetration depth λ. In this regime, strong currents associated with the surface barrier flow and the field distribution and the susceptibility is strongly space inhomogeneous. The influence of these currents on the NMR spectrum is an open question. In addition, if the pairing interaction is modified by magnetic field, the upper critical field can be enhanced above H_{c2}^{P} even in the spin singlet superconductors.

When $\Psi_{\rm pair}(\mathbf{k})$ has an imaginary part

$$\Psi_{\rm pair}(\mathbf{k}) = \psi_1(\mathbf{k}) + {\rm i}\psi_2(\mathbf{k}), \tag{10}$$

the time reversal symmetry is broken, since $\Psi^*_{\rm pair}(\mathbf{k}) \neq \Psi_{\rm pair}(\mathbf{k})$. In such a situation, spontaneous static magnetic field arising from the orbital current around the impurity or at the surface can appear below T_c, because the impurity or boundary lifts the degeneracy between $|L, L_z\rangle$ and $|L, -L_z\rangle$. Such a spontaneous magnetic field was observed in UPt_3 [31], Sr_2RuO_4 [32], and $PrOs_4Sb_{12}$ [33] by μSR experiments.

Recently superconductivity with no spatial inversion symmetry has excited great interest. In the presence of strong spin–orbit interaction, the absence of the inversion symmetry strongly influences the pairing symmetry through a splitting of the two spin degenerate bands. Generally in the system without inversion symmetry the gap function is a mixture of spin singlet and triplet channels in the presence of a finite spin orbit coupling strength. Associated with the absence of spatial inversion symmetry, unusual superconducting properties, including the striking enhancement of H_{c2} and helical vortex phase, have been proposed. The absence of inversion symmetry has been reported in several superconductors. Among them, the superconducting gap function with line nodes have been reported in $CePt_3Si$ [34] and Li_2Pt_3B [35]. In these systems, the position of node is strongly influenced by the mixing of the spin singlet and triplet components.

In table 1, we summarize the gap functions of several anisotropic superconductors. One needs to bear in mind that the gap functions in some of the listed materials are still controversial.

3. Nodal structure: standard techniques

In unconventional superconductors discovered so far, the energy gap for the quasiparticle excitations vanishes (has nodes) at points or along lines on the Fermi surface. There is now a wide variety of dynamic and thermodynamic probes that couple to, and reveal these low energy excitations. The temperature dependence of the London penetration depth $\lambda(T)$, electronic part of the specific heat $C(T)$, thermal conductivity $\kappa(T)$, and nuclear magnetic resonance (NMR) spin–lattice relaxation rate T_1^{-1} all reflect the changes in the quasiparticle occupation numbers. In the fully gapped (s wave) superconductors the quasiparticle density of states (DOS) is zero at energies, E, below the gap edge (no excitations with $E < \Delta$), and varies as $N_s(E)/N_0 = \frac{E}{\sqrt{E^2-\Delta^2}}$ for $E > \Delta$. Here N_0 is the normal state DOS. The physical quantities exhibit activated temperature dependence, $\exp(-\Delta/T)$ at low temperatures, $T \ll T_c$. On the other hand, in nodal superconductors, the low energy density of states remains finite due to contributions from the near nodal regions on the Fermi surface, and typically the DOS varies as $N_s(E)/N_0 = (E/\Delta_0)^n$ at $E \ll \Delta$. The exponent n depends on the topology of the nodes: $n = 1$ for line nodes as well as for point nodes where the gap is quadratic in distance from the nodal point in the momentum space; $n = 2$ for point nodes with linearly varying gap

Table 1. Superconducting gap symmetry of unconventional superconductors. TRS, AFMO and FMO represent time reversal symmetry, antiferromagnetic ordering and ferromagnetic ordering, respectively.

	Node	Parity	TRS	Proposed gap function	Comments
High T_c cuprates	Line (vertical)	Even [7]		$d_{x^2-y^2}$ [7]	
$Sr_2Ca_{12}Cu_{24}O_{41}$	Full gap [25]	Odd [25]			Spin ladder system
κ-$(ET)_2Cu(SCN)_2$	Line (vertical) [66]	Even [148]		d_{xy} [66]	
$(TMTSF)_2PF_6$		Odd [23]			Superconductivity under pressure
$(TMTSF)_2ClO_4$	Line [173] Full gap [181]				
Sr_2RuO_4	Line (horizontal) [65] (vertical) [73]	Odd [24]	Broken [32]	$(k_x + ik_y)\times$ $(\cos k_z c + \alpha)$ [65] $(\sin k_x + i \sin k_y)$ [73]	
$Na_xCoO_2{\cdot}yH_2O$	Line [174]	Even [175, 176], Odd [26, 27]			
(Y, Lu)Ni_2B_2C	Point-like [67]	Even [88]		$1 - \sin^4\theta\cos(4\phi)$ [87, 177]	Very anisotropic s wave
Li_2Pt_3B	Line [35]	Even + odd			No inversion centre
$CeCu_2Si_2$	Line [178]	Even [178]			Two superconducting phases [183]
$CeIn_3$	Line [179]				Coexistence with AFMO
$CeCoIn_5$	Line (vertical)	Even [61]		$d_{x^2-y^2}$ [53, 61, 136], d_{xy} [69]	FFLO phase
$CeRhIn_5$	Line [180]	Even [180]			Coexistence with AFMO
$CePt_3Si$	Line [34]	Even + odd [182]			No inversion centre
UPd_2Al_3	Line (horizontal)	Even [109]		$\cos k_z c$ [62]	Coexistence with AFMO
UNi_2Al_3	Line [19]	Odd [19]			Coexistence with SDW
URu_2Si_2	Line [184]	Odd [20]			Coexistence with hidden order
UPt_3	Line + point [185]	Odd [18]	Broken [31]		Multiple superconducting phases
UBe_{13}	Line [189]	Odd [22]			
UGe_2	Line [186]	Odd [28]			Coexistence with FMO
URhGe		Odd [29]			Coexistence with FMO
UIr		Even + odd [30]			Coexistence with FMO and no inversion centre
$PuCoGa_5$	Line [187]	Even [125]			
$PuRhGa_5$	Line [188]				
$PrOs_4Sb_{12}$	Point [68]	Odd [22]	Broken [33]		Multiple superconducting phases

amplitude around the nodal point. Then the experimental quantities described above exhibit power law temperature dependence at $T \ll T_c$. For example, in d wave superconductors with line nodes, the DOS $N(E) \sim |E|$ leads to the specific heat $C_e \approx \gamma_n T^2/T_c$, where γ_n is the coefficient of the term linear in T in the normal state, and the NMR relaxation rate $T_1^{-1} \propto T^3$. The deviation of the superfluid density, $n_s(T)$ from its zero temperature value, $\Delta n_s(T) = n_s(0) - n_s(T) \propto k_B T/\Delta_0$, which can be detected by the penetration depth measurements.

So far we discussed pure systems. The regime where power laws in T are observed is strongly influenced by the impurities. In unconventional superconductors non-magnetic impurities act as pair breakers, similar to magnetic impurities in s wave superconductors. A bound state appears near an isolated non-magnetic strong (scattering phase shift $\pi/2$, or unitarity) scatterer, at the energy close to the Fermi level. The broadening of this bound state to an impurity band at finite disorder leads to a finite density of states at zero energy, $N(0)$, that increases with increasing impurity concentration [36]. The impurity scattering changes the temperature dependence of the physical quantities below T corresponding to the impurity bandwidth: $\Delta\lambda$ changes the behaviour from T to T^2, the NMR relaxation rate changes from $T_1^{-1} \propto T^3$ to $T_1^{-1} \propto T$ ($T_1 T \sim$ const), and $C(T)$ changes from T^2 to T. In NMR, for example, the temperature range where T_1^{-1} exhibits the T^3 dependence is limited to $T > T_c/3$ in most measurements.

Therefore the nodal behaviour may be hidden by the impurity effects. Even in the extremely pure systems, however, experimental observation of the power laws provides indications of the existence of the nodes, but is unable to yield information about their location in the momentum space.

Angle resolved photoemission spectroscopy (ARPES) directly investigates the momentum dependence of the gap, and was instrumental in determining the gap shape in high T_c superconductors. However, the energy resolution of this technique is insufficient when compared with the size of the energy gap in most low T_c systems. The phase sensitive measurements, such as for corner junctions, tricrystal, and tests for Andreev bound states, which provided the most convincing evidence for $d_{x^2-y^2}$ wave order parameter in the high T_c cuprates, are primarily surface probes. Absence of inversion symmetry near the surface may influence the pairing symmetry through, for example, splitting of the two spin degenerate bands via the spin–orbit coupling, so that the gap function is a mixture of the spin singlet and spin triplet channels. Moreover, it is difficult to apply these techniques to determine the three dimensional gap structure, and they have received limited use beyond studies of the high T_c cuprates. It is therefore extremely important to acquire complementary evidence for particular gap symmetries via bulk measurements.

4. Nodal superconductor in a magnetic field

4.1. General approaches to the vortex state

Determining the nodal positions requires a directional probe. In the following we argue that an applied magnetic field provides a convenient bulk probe of the symmetry of the order parameter in unconventional superconductors. The usefulness of the magnetic field as a probe relies on an important difference between the properties of the vortex state in nodal compared to fully gapped s wave superconductors. While for the s wave case the DOS and the entropy at low fields, $H \ll H_{c2}$, are determined by the localized states in the vortex cores, in the superconductors with nodes they are dominated by the extended quasiparticle states, which exist in the bulk close to the nodal directions in momentum space. Therefore much attention has been paid to the effect of the field on these near nodal quasiparticle.

A simple picture that captures the main effect of the magnetic field on a nodal superconductor is that of the Doppler shift of the quasiparticle spectrum [37]. In the presence of a supercurrent with velocity $\mathbf{v}_s$ the energy of a quasiparticle with momentum $\mathbf{k}$ is Doppler shifted relative to the superconducting condensate by

$$\varepsilon(\mathbf{k}) \to \varepsilon(\mathbf{k}) - \hbar\mathbf{k}\cdot\mathbf{v}_s. \tag{11}$$

This effect originates from the Galilean transformation: creation of an excitation $(\mathbf{p}, \varepsilon)$ in the rest frame of the normal quasiparticle, involves an additional energy $\delta\varepsilon = \mathbf{p}\cdot\mathbf{v}_s$ in the superfluid frame of reference. For a uniform superflow the Doppler shift is simply a consequence of the gauge invariance, and is therefore exact [38]. For a non-uniform superflow, as in the vortex state, this picture is semiclassical in that it considers simultaneously the momentum of the quasiparticles and the local value of $\mathbf{v}_s(\mathbf{r})$ at position $\mathbf{r}$, and therefore ignores the possible accumulation of the quantum mechanical phase around the magnetic vortices in superconductors. The fully quantum mechanical treatment of the quasiparticle energies so far was carried out only in a perfectly periodic vortex lattice and in the absence of impurities [39], and gives results for the physical properties close to those obtained in the semiclassical treatment [39, 40].

To estimate the characteristic energy scale of the Doppler shift we can approximate the velocity field by that around a single vortex, $\mathbf{v}_s = \hbar\hat{\phi}/2mr$, where r is the distance from the centre of the vortex and $\hat{\phi}$ is a unit vector along the circulating current. This expression is valid outside the vortex core and up to a cut-off of order $\min\{R, \lambda\}$, where $R = a\sqrt{\Phi_0/\pi H}$ is the intervortex distance, Φ_0 is the flux quantum, a is a geometric constant, and λ is the London penetration depth. Average Doppler shift, E_{av}, is computed by integrating over a vortex lattice unit cell, and is given by

$$E_{\mathrm{av}} = \langle|\mathbf{v}_s\cdot\mathbf{p}|\rangle = \int_{|\mathbf{r}|<R}\frac{\mathrm{d}^2\mathbf{r}}{\pi R^2}|\mathbf{p}\cdot\mathbf{v}_s| \approx \frac{4}{a\pi}\hbar v_F\sqrt{\frac{H}{\Phi_0}}. \tag{12}$$

Thus E_{av} is proportional to $\sqrt{H}$.

Since the density of states is an additive quantity, the net DOS of the sample is the sum of the contributions from the areas with distinct values of the Doppler shift. In a system with line nodes, where the low energy DOS $N(E) \propto |E|$, this implies the residual density of states $N_v(E = 0, H) \propto E_{\mathrm{av}} \propto \sqrt{H}$. Consequently the specific heat also exhibits the $\sqrt{H}$ behaviour at low temperatures in the clean limit [37, 41–43]. Since the supervelocity distribution can be obtained for a given configuration of vortices, the range of possible values for the coefficient of the $\sqrt{H}$ can also be found for a given material [44].

Determining the transport properties, such as the thermal conductivity κ, using the Doppler shift method is a more challenging task. The transport coefficients are determined from the correlation functions that have a finite range, and therefore depend on the Doppler shift at more than a single point. Local values of these coefficients can be rigorously defined only in the dirty limit. It is generally accepted that a similar definition gives at least a qualitatively correct results in the clean limit [45], although a rigorous comparison is currently lacking. Even with that assumption, the connection between the distribution of local values, $\kappa(\mathbf{r})$, and the measured value remains a subject of some debate. Both averaging $\kappa(\mathbf{r})$ and $\kappa^{-1}(\mathbf{r})$ have been proposed [45, 46]. While in some cases the difference is only in the magnitude of the field induced change, the divergent philosophies behind the averaging procedures give rise to qualitatively different results for the anisotropy of the transport coefficients described below.

In the approach discussed above only the quasiparticle energy is shifted, so that the single particle scattering rate is not directly affected by the presence of the vortices. In the presence of static disorder treated, for example, in the self-consistent T-matrix approximation, the

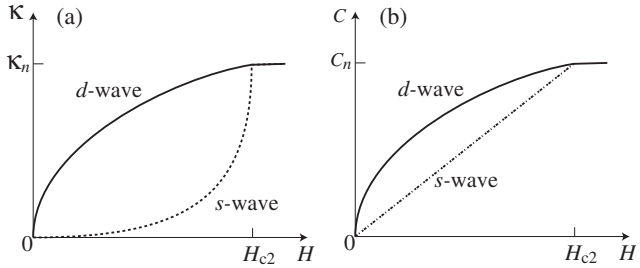

Figure 1. Field dependence of (a) the thermal conductivity κ and (b) the specific heat C for s and d wave superconductors. In s wave superconductors, the thermal conductivity shows an exponential behaviour with very slow growth with H [54, 55]. The heat capacity increases nearly linearly with H. In sharp contrast, in d wave superconductors, both the specific heat and the quasiparticle conduction grows rapidly as soon as the field exceeds H_{c1}. The slope of $\kappa(H)$ at H_{c2} depends on purity and therefore for the d wave case it is also possible to have an inflection point in $\kappa(H)$ at intermediate fields.

magnetic field does affect the lifetime indirectly, by modifying the density of states available for scattering [41, 45]. Hence the Doppler shift method does not account for scattering of the quasiparticles on vortices.

Calculations of the vortex scattering cross-section have to go beyond the semiclassical treatment and make assumptions about the structure of the vortex core states [47], and therefore received limited attention. An alternative, fully microscopic approach, employs an extension of the approximation originally due to Brandt, Pesch and Tewordt (BPT) [48, 49] to describe clean superconductors near the upper critical field, H_{c2}. In this method the Gor'kov equations (or their quasi-classical Eilenberger–Larkin–Ovchinnikov analogue) are solved with the normal electron Green's function replaced by its spatial average [49–53]. This method is rigorously justified at moderate to high fields, gives the standard quasiparticle spectrum as $H \to 0$, and yields results that are qualitatively similar to the Doppler shift at very low fields and temperatures. Therefore it is believed that it can be used over a wide range of fields relevant to experiment. The BPT approach naturally includes the scattering of the quasiparticles off the vortices [50, 53]; however, due to the incoherent averaging over different unit cells of the vortex lattice, it tends to overestimate the importance of such scattering at lower fields. Together, BPT and Doppler shift methods account for a majority of theoretical work relevant to the experimental investigations of the quasiparticle properties in the vortex state of nodal superconductors.

4.2. Thermal conductivity

Of all the transport properties the thermal conductivity is uniquely suitable for probing bulk superconductivity. Unlike electrical resistivity, it does not vanish in the superconducting state. Cooper pairs do not carry entropy and therefore do not contribute to the thermal transport. As a result, the thermal conductivity probes the delocalized low energy quasiparticle excitations, and is sensitive to the effect of magnetic field on the quasiparticles. In figure 1 we show the qualitative behaviour of the thermal conductivity and heat capacity at low T as a function of the magnetic field for an s wave (fully gapped) and a d wave (with line nodes) superconductor.

In s wave superconductors the only quasiparticle states present at $T \ll T_c$ are those associated with vortices. At low fields where the vortices are far apart, these states are bound to the vortex core and are therefore localized and unable to transport heat; the thermal

conductivity shows an exponential behaviour with very slow growth with H. At high fields near H_{c2} where quasiparticles states within the vortices begins to overlap with those within the neighbouring vortices, thermal conductivity increases rapidly. Such a field dependence of the thermal conductivity is observed in Nb [54, 55]. The heat capacity, due to the localized quasiparticle states, increases nearly linearly with H. In dramatic contrast, both the specific heat and the quasiparticle conduction, due to near nodal states, grow rapidly as soon as the field exceeds H_{c1}. In d wave superconductors where $N(E = 0, H) \propto \sqrt{H}$ due to the Doppler shift of the quasiparticle energy spectrum, both the thermal conductivity and the specific heat exhibit a nearly $\sqrt{H}$ behaviour.

In reality, especially at higher temperatures, the behaviour of the thermal conductivity is more complex. While the magnetic field enhances the local DOS, it also leads to a change in the transport lifetime both via the modification of the impurity scattering and via Andreev scattering off the vortices. Understanding of these competing effects has progressed during the past few years [44, 45, 50, 53, 56–59], although the complete picture is not yet developed. In general, at low temperatures the DOS modification plays the dominant role, and the thermal conductivity increases with increased field. At higher temperatures and low fields, the dominant effect of vortices is to introduce and additional scattering mechanism, while the DOS is controlled by T. Consequently, the thermal conductivity initially decreases with field, and goes through a minimum at a finite H [50]. This behaviour has been first observed in high T_c cuprates [60], and also seen in other systems [61, 62].

5. How do we determine the nodal structure in the bulk?

5.1. Anisotropy under a rotating field: density of states

The techniques described above help determine the general topology of the gap, but cannot establish the exact angular dependence of $\Delta(\mathbf{k})$. In particular, the nodal positions in $\mathbf{k}$-space cannot be obtained. In the following we discuss the theoretical underpinnings and experimental realizations of the new and powerful method for determining the nodal directions.

The method is based on the prediction that, under an applied magnetic field, the density of states of nodal superconductors depends on the orientation of the field with respect to the nodal direction [63], and exhibits characteristic oscillations as the field is rotated relative to the sample. The oscillations can be measured via the field-angle dependence of the thermal conductivity [58, 59, 61, 62, 64–68] or specific heat [69–73].

While the specific heat measurements directly probe the density of states, the thermal conductivity anisotropy is sensitive to a combination of the density of states, and the quasiparticle transport scattering rate, which may have different dependence on the field orientation. Measurements of the specific heat anisotropy were only attempted several years after theoretical predictions [69–73]. First experiments on the field-angle dependence of the thermal conductivity preceded theoretical discussions [58, 59], but focused simply on the existence, rather than location, of additional features (interpreted as arising from Andreev scattering) in cuprates. Use of the thermal conductivity as a similar test based on the DOS anisotropy was, to our knowledge, first suggested in [74], and followed up by other work [46]. Development and consistent use of the measurements to probe the direction and type of nodes in $\mathbf{k}$-space, is almost entirely due to recent efforts by the group of University of Tokyo [61, 62, 65–68]. The full theory of the anisotropy of the thermal conductivity in the vortex state is still incomplete. Hence, while the salient features of experiments are qualitatively understood based on a number of treatments [46, 53, 63, 75–83], many details need to be addressed further. Below we discuss the current status of this field.

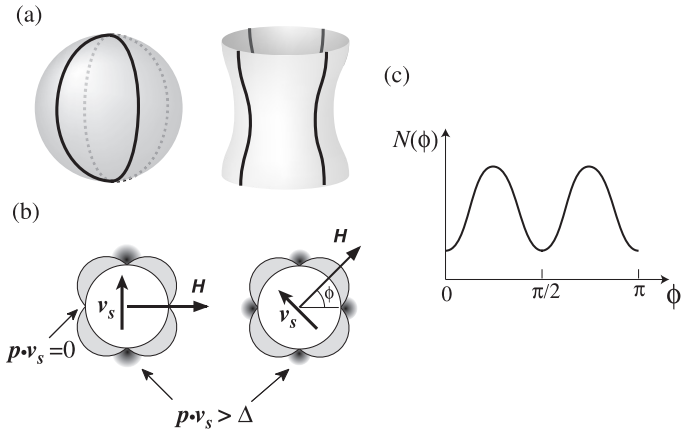

Figure 2. (a) Sketch of the gap structure with four line nodes perpendicular to the basal plane (vertical node). (b) Schematic diagram showing the regions on the Fermi surface that experience the Doppler shift in **H** within the basal plane. We have assumed d_{xy} symmetry. $\phi = (\mathbf{H}, a)$ is the azimuthal angle measured from the a axis. With **H** applied along the antinodal directions, all four nodes contribute to the DOS, while for **H** applied parallel to the node directions, the Doppler shift vanishes at two of the nodes. (c) Fourfold oscillation of the DOS for **H** rotating in the basal plane. The DOS shows a maximum (minimum) when **H** is applied in the antinodal (nodal) direction.

The origin of the anisotropy is best understood in the framework of the Doppler shift of the delocalized quasiparticle spectrum in the vortex state. Consider, for simplicity, a d_{xy} gap symmetry with four vertical lines of nodes, and assume a cylindrical or spherical Fermi surface, as illustrated in figures 2(a)–(c). At low fields, the loci of unpaired quasiparticles in the momentum space are close to the nodal lines. Since the supercurrents flow in the plane normal to direction of the applied field, the Doppler shift experienced by quasiparticles in a given near nodal region depends on the direction of the field $\mathbf{H}(\theta, \phi) = H(\sin\theta\cos\phi, \sin\theta\sin\phi, \cos\theta)$ with respect to the nodal directions. Here θ and ϕ are the polar angle and the azimuthal angle respectively, measured relative to the c axis.

Consider **H** rotated conically (fixed θ) with varying in-plane angle, ϕ; see the view from above in figure 2(b). When the field is aligned with a nodal line, the superflow around the vortices is in the plane nearly normal to the momenta of quasiparticles close to that node. As a result, for these quasiparticles the Doppler shift is small. In contrast, when the field is in the antinodal direction, the Doppler shift is (relatively) large along all four nodal lines. As a result, the net DOS has minima when **H** is aligned with the nodal direction, and maxima for **H** along the antinodes [63]. The angle dependence of the DOS exhibits characteristic fourfold oscillations, as shown in figure 2(c). In general, the DOS oscillates with n-fold symmetry corresponding to the number of vertical nodes n.

In this approach the amplitude of the DOS oscillations, $\delta N(E)/N(E)$, depends on the shape of the Fermi surface and other parameters of the models. For the residual ($E = 0$) DOS, most calculations predict the oscillation amplitude ranging from 3% to 10%. The anisotropy is rapidly washed away at finite energy, and therefore the amplitude of the corresponding oscillations in the measured quantities, such as the specific heat, at finite temperature, is typically of the order of a few per cent.

Consider now horizontal line nodes in a cylindrical or spherical Fermi surface, as illustrated in figure 3(a). The density of states is anisotropic under the rotation of the field in the ac plane, by varying the angle θ. To illustrate the difference between the line nodes

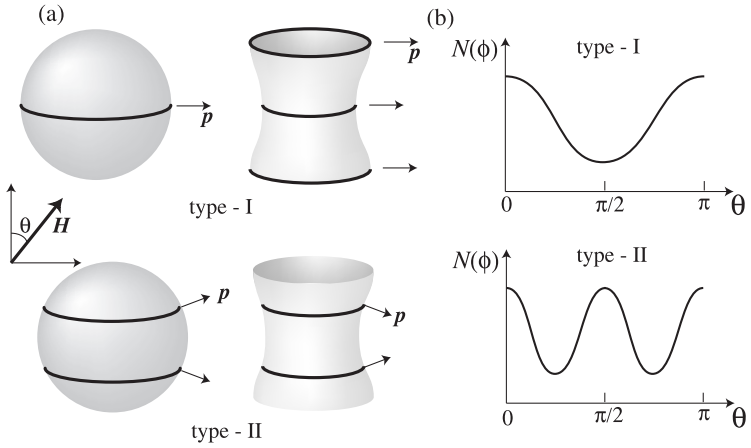

Figure 3. (a) Schematic diagram of the gap structure with line nodes parallel to the basal plane (horizontal node) in spherical and open Fermi surfaces. Type I assumes a gap function $\Delta(\mathbf{k}) \propto \sin k_z c$, where line nodes are located at the centre of the Brillouin zone and at the zone boundary. Type II assumes a gap function $\Delta(\mathbf{k}) \propto \cos k_z c$, where line nodes are located at positions shifted off the zone centre. (b) Oscillations of the DOS for **H** rotating in the *ac* plane for various gap functions. Twofold oscillation with the same sign are expected for type I. On the other hand, for type II, an oscillation with a double minimum is expected.

at high symmetry positions in the Brillouin zone, and away from those, we consider here two model gap functions

(i) Type I: horizontal nodes located at the centre of the Brillouin zone and at the zone boundary $\Delta(\mathbf{k}) \propto \sin k_z c$.
(ii) Type II: horizontal nodes located at positions shifted off the zone centre; $\Delta(\mathbf{k}) \propto \cos k_z c$.

The expected angular variation of the Doppler shifted DOS is a function of the relative angle between **H** and **p** for these gap functions, this is shown schematically in figure 3(b). The twofold oscillation is expected for type I gap functions, in which the horizontal nodes are located at the position where $\mathbf{p} \parallel ab$ plane. On the other hand, for type II, one expects an oscillation with a double minimum structure as a function of θ. Note that we sketched the DOS for a fixed H/H_{c2}; if a measurement is done at a fixed H, the anisotropy of H_{c2} in a quasi-2D systems superimposes an additional twofold component on the oscillations, so that for a type II gap the central maximum is distinct from the other two.

The Doppler shift method does not account for the scattering of electrons on vortices. Fully microscopic analyses indicate that inclusion of such scattering further reduces the amplitude of the DOS anisotropy [44]. Furthermore, it has been shown very recently that at moderate to high fields and temperatures the vortex scattering leads to the inversion of the anisotropy: the density of states is greater for the field along the nodal directions than for the field along the gap maxima [53]. While this makes the analysis of the specific heat data more complicated, it affects the conclusions drawn from the analysis of the transport properties less dramatically [53], as we discuss in the next section.

5.2. Anisotropy under a rotating field: thermal conductivity

Our focus in this review is on the determination of the nodal structure via the thermal conductivity measurements. The anisotropy of transport coefficients is given by a combined

effect of the angular variations of the density of states, and the angle dependent scattering. The latter effect is not yet fully understood. Since in self-consistent treatments the scattering rate of quasiparticles off impurities depends on the density of states, the impurity scattering under a rotating field acquires the same n-fold anisotropy as the DOS. However, depending on the strength of impurity scattering, temperature, and the field, the lifetime may exhibit either maxima or minima for the field aligned with the nodes. Consequently, the possibility of the inversion of the maxima and minima in the T–H superconducting phase diagram (which was unexpected in the behaviour of the DOS and the specific heat) was anticipated in the anisotropy of the transport coefficients.

It is believed that the field dependence of the thermal conductivity indicates whether the lifetime or the density of states effects dominate. In the regime where $\kappa(H)$ decreases with increasing field due to field-enhanced scattering, the maxima of the anisotropic conductivity are likely to correspond to nodal direction. In contrast, when $\kappa(H)$ increases with field, the density of states effects dominate, and the minima of the n-fold pattern indicate the nodes. This conjecture is not rigorous [53], but qualitatively correct and provides guidance in the situations when no results of microscopic theory are available for a given compound. Moreover, in experiment the angle induced anisotropy of $\kappa(H)$ changes sign close to the point where the field dependence has a minimum, supporting this view.

When a heat current, $\mathbf{j_h}$, is applied in the basal plane, the angle between $\mathbf{j_h}$ and $\mathbf{H}$ is varied as the field is rotated. Consequently, the dominant anisotropy observed in experiment is that between the transport along and normal to the vortices, i.e. twofold [84]. The nodal contribution appears as a smaller effect on this background, as was first seen in the high T_c cuprate $YBa_2Cu_3O_{7-\delta}$ [58, 59, 64]. Note that with few exceptions [85] Doppler shift does not describe the combined twofold and nodal anisotropy.

More sophisticated approaches based on the BPT theory give correct shapes of the $\kappa(\phi)$ curves, and account for most of the observed features. The details of the competition between the twofold and the fourfold oscillations depend on the shape of the Fermi surface, role of Zeeman splitting, impurity strength and concentration etc. Therefore any semiquantitative comparison of theory and experiment requires knowledge of these as an input, and has only been done for few systems. At the same time qualitative conclusions about the shape of the gap can still be drawn from the simplified analysis, and we review those for the specific compounds discussed below.

For relatively three dimensional systems, the current can be applied along the c axis, and the field rotated conically, varying the azimuthal angle ϕ, and keeping the polar angle θ constant. In that case the relative orientation of the heat current and the field remains unchanged, and the oscillations reflect solely the nodal structure. Vortex scattering still modifies the amplitude and the sign of these oscillations, but the interpretation is greatly simplified by the absence of the dominant twofold term.

In this geometry it has been predicted that the θ dependence of the shape and the amplitude of the periodic oscillations provide direct information on the type of nodes, point or line [67]. In figures 4(a) and (b), we compare the angular variation of the thermal conductivity κ_{zz} (the heat current $\mathbf{q} \parallel z$) when the magnetic field is rotated conically as a function of ϕ, keeping θ constant, for two different types of nodes calculated from the Doppler shifted QP spectrum, in accordance with [67]. Here we adopted gap functions $\Delta(\mathbf{k}) = \Delta_0 \sin(2\phi)$ (d wave) for line nodes, and $\Delta(\mathbf{k}) = \frac{1}{2}\Delta_0\{1 - \sin^4\theta\cos(4\phi)\}$ for point nodes. The latter was proposed in [86], but is probably not realized in this system, and we use it as a convenient ansatz to illustrate the behaviour due to point nodes. These gap functions are illustrated in the insets of figures 4(a) and (b). Here the clean limit $\frac{\hbar\Gamma}{\Delta} \ll \frac{H}{H_{c2}}$ is assumed, where Γ is the carrier scattering rate.

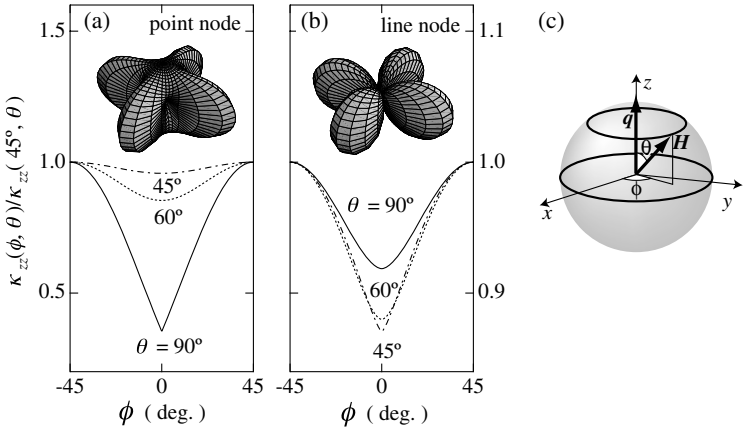

Figure 4. The thermal conductivity $\kappa_{zz}(\phi, \theta)$ (the heat current $\mathbf{q} \parallel z$) when the magnetic field is rotated conically as a function of ϕ, keeping θ constant, for two different types of nodes, (a) point and (b) line. $\kappa_{zz}(\phi, \theta)$ is normalized by $\kappa_{zz}(45°, \theta)$. The corresponding gap functions are illustrated in the insets. (c) Definition of θ (polar angle) and ϕ (azimuthal angle). After [87]. Note that for vertical line nodes the relative amplitude of oscillations for θ between 45° and 90° depends on the shape of the Fermi surface, not accounted for in [87].

According to the Doppler shift picture, there are two major differences in the angular variation of the thermal conductivity between point nodes and line nodes. First, the shape of the $\kappa(\phi)$ curves is different. While the oscillation is close to a sinusoidal wave for line node (figure 4(b)), a narrow cusp structure is predicted for the point node at $T = 0$ (figure 4(a)). Qualitatively, the cusp appears as a result of the small phase space available for the quasiparticles induced in the vicinity of point nodes by the applied field. For line node the corresponding phase space is greater, and the minimum is not as sharp. Second, the amplitude of the oscillation at $T = 0$ decreases rapidly when the $\mathbf{H}$ is rotated conically as a function of ϕ keeping θ constant. For point nodes, the amplitude of the oscillation of the thermal conductivity at $\theta = 45°$ is much smaller than that at $\theta = 90°$, while they are of almost the same magnitude for line nodes. This can be accounted for considering the fact that for $\theta = 45°$ geometry the field $\mathbf{H}$ is never aligned with the point nodes on the equator. Hence there is always a finite Doppler shift at all the nodes. In contrast, for vertical line nodes, the rotating $\mathbf{H}$ at any θ always crosses the line of nodes leading to a greater suppression of the DOS.

While no microscopic calculations exist at present for this geometry, it is likely that the main conclusions of the Doppler shift picture remain valid. As discussed above, the salient features of the measurement in the conical experimental geometry are less sensitive to the vortex scattering than those measured with the heat current in the basal plane. It is likely that the sharp cusp is smeared by finite temperature, but the rapid decay of the oscillations as the field is tilted away from the plane must remain observable. Nonetheless, more work utilizing microscopic theory is clearly desirable in this situation.

In summary, the variation of the field direction in (θ, ϕ) leads to periodic variations in both the thermal conductivity and the heat capacity of nodal superconductors. From the periodicity, phase and shape of the angular variation of the thermal conductivity and heat capacity, one can extract information on the direction and type of nodes in $\mathbf{k}$-space.

5.3. Experimental procedure

In the experiments described below the thermal conductivity was measured in a ^{3}He cryostat by using the standard steady-state method, with a heater and two carefully calibrated RuO_2

thermometers. In all the measurements, and especially in quasi-2D superconductors with very anisotropic upper critical field, it is critically important to align **H** in the plane with high accuracy, and have a good control over its rotation. Even a slight field misalignment may produce a large effect on the measured κ, influencing the conclusions. To achieve this high precision for the orientation of **H** relative to the crystal axes, we used a system with two superconducting magnets generating magnetic fields in two mutually orthogonal directions, and a ^{3}He cryostat set on a mechanical rotating stage at the top of a Dewar. By computer controlling the two superconducting magnets and rotating stage, we were able to rotate **H** with a misalignment of less than 0.02° from each axis, which we confirmed by simultaneous measurements of the resistivity.

Since the thermal conductivity can be measured both under the field $\mathbf{H} = H(\sin\theta\cos\phi, \sin\theta\sin\phi, \cos\theta)$ rotated within the basal ab plane (as a function of ϕ at $\theta = 90$), and **H** rotated as a function of θ at fixed ϕ, we were able to detect both vertical and horizontal nodal structure. In addition, measuring the thermal conductivity with $\mathbf{H} = H(\sin\theta\cos\phi, \sin\theta\sin\phi, \cos\theta)$ rotated conically as a function of ϕ, keeping θ constant, as shown in figure 4, enables us, at least in principle, to distinguish line and point nodes. In the following we discuss the experimental results for different compounds.

One of the recurring aspects of the discussion is the relative importance of electron and phonon (or spin wave) contributions to the net thermal conductivity. While at low temperatures the bosons are less efficient than fermions in carrying heat, in systems with significant spin fluctuations or low carrier density the bosonic degrees of freedom may be dominant over a wide T–H range. Since only electrons carry charge current, we take the point of view that if the measured Wiedemann–Franz ratio of the thermal to electrical conductivities, $L = \kappa_{zz}\rho_{zz}/T$, just above T_c is close to the Lorenz number $L_0 = 2.44 \times 10^{-8}\ \Omega\ \mathrm{W\ K^{-1}}$, obtained under assumption of purely electronic κ, the electronic contribution to the thermal conductivity is dominant. Even though, strictly speaking, in the presence of inelastic scattering, $L \to L_0$ only as $T \to 0$, quite generally opening of an additional bosonic conduction channel increases L compared to L_0, and has clear experimental signatures.

In several of the systems we discuss $\kappa(T)/T > \kappa(T_c)/T_c$ at least in some range $T \lesssim T_c$ and often has peak at $T^\star < T_c$. In compounds with low carrier density, and therefore with thermal transport dominated by bosonic degrees of freedom, this may be due to increased mean free path of phonons as the unpaired electron density is decreased. In other materials, such increase is due to rapid reduction of the inelastic scattering rate below T_c (faster than the concomitant reduction in the electron density of states). In some systems, the two effects combine. Generally, a comprehensive analysis of a large body of data on a given compound provides a clue to what mechanism is more important. We indicate this for each of the materials analysed below.

6. Three dimensional unconventional superconductors

6.1. Borocarbide YNi_2B_2C

We start by considering the superconducting gap structure of a non-magnetic borocarbide superconductors $LnNi_2B_2C$, Ln = (Y and Lu) [12]. These systems have tetragonal crystal symmetry, and the electronic band structure is essentially 3D; see figure 5. Early on, these materials were assumed to have an isotropic s wave gap, similar to most compounds where superconductivity is mediated by conventional electron–phonon interactions. However, recent experimental studies, such as specific heat [88, 89], thermal conductivity [90], Raman scattering [91], and photoemission spectroscopy [92] on YNi_2B_2C or $LuNi_2B_2C$ have reported

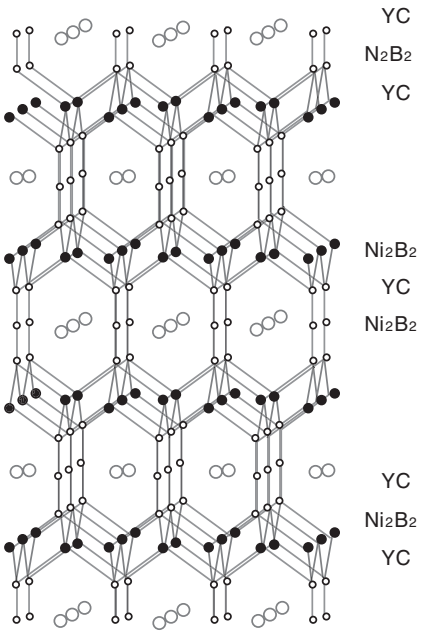

Figure 5. Crystal structure of YNi_2B_2C.

a large anisotropy in the gap function. Below we review the implications of the thermal conductivity measurements for the gap symmetry.

Figure 6(a) shows the T dependence of the c axis thermal conductivity κ_{zz} (the heat current $\mathbf{q} \parallel c$) of YNi_2B_2C ($T_c = 15.5$ K) single crystal with no magnetic field. The residual resistivity ratio of this crystal is approximately 47 (the highest crystal quality currently achievable). Upon entering the superconducting state, κ_{zz} exhibits a small kink, as expected for a second order transition. The Wiedemann–Franz ratio at T_c, $L = \kappa_{zz}\rho_{zz}/T \simeq 1.02L_0$ indicating that the electronic contribution to κ is dominant. The inset of figure 6(a) shows the same data below 1 K, where the T dependence of κ_{zz} is close to quadratic (rather than cubic, as it would be for dominant phonon contribution). Figure 6(b) depicts the magnetic field dependence of κ_{zz} ($\mathbf{H} \parallel [110]$) at low temperatures. Rapid increase of κ_{zz} at low fields is markedly different from that observed in typical s wave materials [54]. This steep increase of the thermal conductivity, along with the $\sqrt{H}$ dependence of the heat capacity [88, 89], strongly suggests that the thermal properties are governed by the delocalized QPs arising from the nodes (or extremely deep minima) in the gap.

Having established the predominant contribution of the extended QPs in the thermal transport, we are in the position to address the nodal structure of the gap function. As discussed above, in three dimensional systems, conical rotation of the field allows a more direct observation of the nodal structure. Figure 7 displays the angular variation of κ_{zz}, measured by rotating $\mathbf{H} = H(\sin\theta\cos\phi, \sin\theta\sin\phi, \cos\theta)$ conically, as a function of ϕ, at a constant θ. The measurements were done by rotating ϕ after field cooling at $\phi = -45°$. The open circles in figure 7 show $\kappa_{zz}(H, \phi)$ at $H = 1$ T which are obtained under the field cooling at each angle, and demonstrate excellent agreement between the two sets of measurements. A clear fourfold symmetry is observed for the ϕ rotation at $\theta = 90°$ and $60°$, so that $\kappa_{zz} = \kappa_{zz}^0 + \kappa_{zz}^{4\phi}$. Here κ_{zz}^0 is ϕ independent, and $\kappa_{zz}^{4\phi}$ has the fourfold symmetry with respect to ϕ rotation.

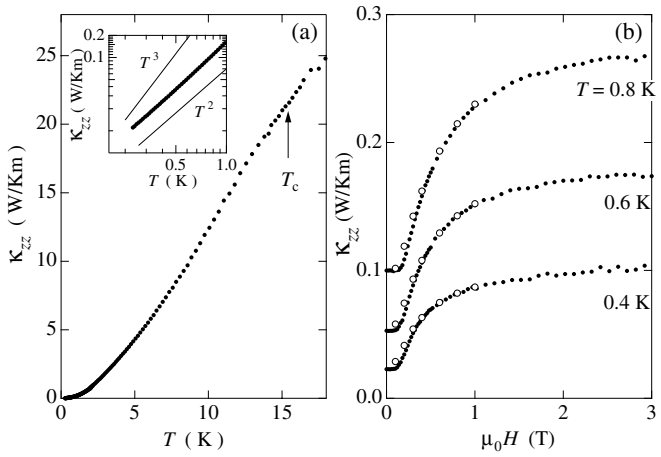

Figure 6. (a) Temperature dependence of the c axis thermal conductivity κ_{zz} in zero field. Inset: log–log plot of the same data below 1 K. (b) Field dependence of κ_{zz} at low temperatures (**H** ∥ [110]). The solid circles represent the data measured by sweeping H after zero field cooling, and the open circles represent the data measured under field cooling conditions at each temperature.

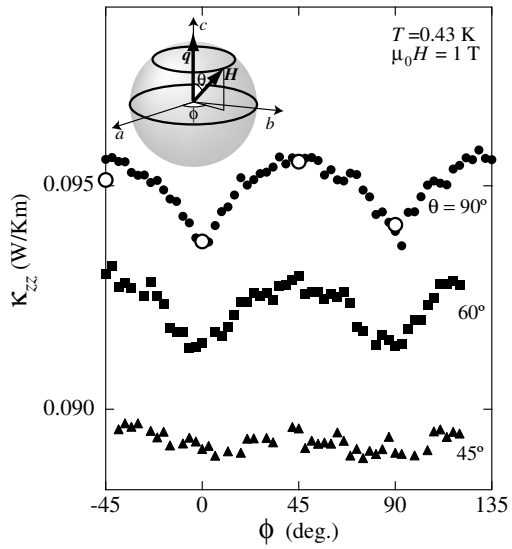

Figure 7. Angular variation of κ_{zz} (**q** ∥ c), measured by rotating $\mathbf{H}(\theta, \phi) = H(\sin\theta\cos\phi, \sin\theta\sin\phi, \cos\theta)$ conically as a function of ϕ at fixed $\theta = 90°, 60°$, and 45° (see the inset). The open circles represent the data obtained under the field cooling condition at each angle.

As seen in figure 7, $\kappa_{zz}^{4\phi}$ has a narrow cusp at $\phi = 0°$ and 90°. We stress that the anisotropies of the Fermi velocity v_F and H_{c2}, which are inherent to the tetragonal band structure of YNi_2B_2C, are unlikely to be at the origin of the observed fourfold symmetry. The fourfold ϕ dependence of H_{c2} at $\theta = 90°$ and 45° is nearly perfectly sinusoidal [93], and therefore different from the ϕ dependence of $\kappa_{zz}^{4\phi}$ displayed in figure 7. According to the previous section, the minima of $\kappa_{zz}^{4\phi}$ at $\phi = 0°$ and 90° immediately indicate that *the nodes are located along [100] and [010] directions*.

The cusp structure and the θ dependence of $\kappa_{zz}^{4\phi}$ are key features for specifying the type of nodes. First, the cusp itself is markedly different from the smooth (almost sinusoidal) feature predicted (see the previous section, figure 4) and observed (see the next section) in superconductors with line nodes, such as d wave. Second, the amplitude of $\kappa_{zz}^{4\phi}$ decreases rapidly as **H** is changed from the in-plane $\theta = 90°$ to 45°. Therefore direct comparison of the data on both the cusp structure and θ dependence of κ_{zz} with figure 4 strongly favours a model with point nodes, and leads us to conclude that the superconducting gap function of YNi_2B_2C has *point nodes* along [100] and [010] directions.

For a gap with point nodes the T dependence of the thermodynamic quantities at low temperature depends on whether the gap increases linearly or quadratically with the distance from the nodal point. *The gap function we used predicts a quadratic T dependence of the thermal conductivity, which is consistent with the data in the inset of figure* 6(a).

More recent measurements of the angular variation of the heat capacity also report the fourfold oscillations consistent with the present experiments [70]. Very recent STS measurements in the vortex state of YNi_2B_2C have demonstrated the presence of the extended QPs in the [010] direction [94]. Thus the nodal structure is confirmed by the several different techniques.

Are these real nodes or simply deep minima? Experimentally, a clear fourfold pattern is seen at $T = 0.27$ K and $H = 1\ T \sim 0.1 H_{c2}$. This suggests that the typical Doppler energy, $E_{av} \sim \Delta_0 \sqrt{H/H_{c2}}$, of the nodal quasiparticles far exceeds both T, and the minimal gap Δ_{min}. Here we estimate $\Delta_0 \sim \hbar v_F/\pi\xi_0$. This leads to the anisotropy ratio $\Delta_{min}/\Delta_0 \ll 0.3$. A more stringent constraint may be deduced from the power law temperature dependence of the thermal conductivity down to this temperature in zero field. Estimating, $\Delta_0 \sim 28$ K from the value of T_c, we find $\Delta_{min}/\Delta_0 \lesssim 0.01$.

While this value is small, the origin of the true nodes is topological, and hence the important question is whether the gap function changes its sign on the Fermi surface. To answer it, we examined the impurity effect on the gap anisotropy. In an anisotropic s wave superconductor, with accidental gap minima or zeros, introduction of non-magnetic impurities affects T_c only moderately, and rapidly makes the gap more isotropic thereby reducing the DOS at the Fermi surface by removing the node. On the other hand, if the gap changes sign and its average over the Fermi surface vanishes, doping with impurities suppresses T_c more severely, and induces a finite DOS at energies smaller than the scattering rate, γ. In the latter case the oscillations of $\kappa(H)$ persist in the regime where the Doppler energy $\gamma \lesssim E_{av}$.

Figure 8 shows the absence of the angular variation of the thermal conductivity $\kappa_{zz}(\theta = 90°, \phi)$ in the Pt-substituted compound $Y(Ni_{1-x}Pt_x)_2C$ with $x = 0.05$. We estimate that $E_{av} \sim 0.3\Delta_0$. On the other hand, the transition temperature changes little with Pt doping [88, 95]. Then the disappearance of the angular variation in κ indicates the opening of the gap, and the destruction of nodal regions by impurity scattering. This is consistent with the heat capacity measurements, which reports a transition from $\sqrt{H}$ behaviour of $\gamma(H)$ at $x = 0$ to linear in H behaviour for $x = 0.2$ [88].

It has been pointed out that the cusp structure in the angular variation of the thermal conductivity can appear as a result of the nesting property of the Fermi surface [80]. However, the disappearance of the angular variation in $Y(Ni_{1-x}Pt_x)_2C$ with $x = 0.05$, indicates that this scenario is unlikely. Moreover the cusp structure appears even in $ErNi_2B_2C$, in which the nesting part of the Fermi surface disappears due to the spin density wave transition [96].

Therefore, comparison of the experiment with existing theories yields the gap structure with point nodes. While these may be accidental, an alternative view is that a strong Coulomb repulsion is an essential ingredient of the models required for the borocarbides. Recently, it has been shown that the s wave superconductivity with deep gap minimum appears when the

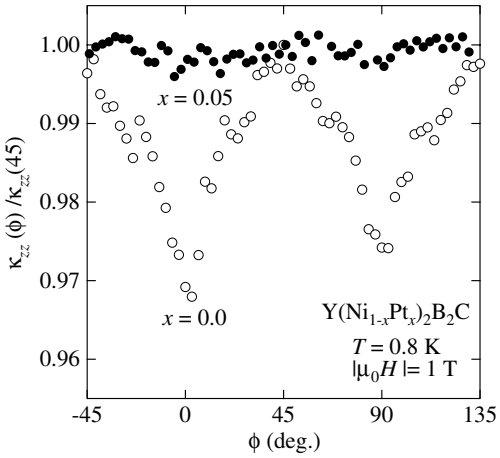

Figure 8. Angular variation of κ_{zz} for YNi_2B_2C (open circle) and $Y(Ni_{0.95}Pt_{0.05})_2B_2C$ (solid circles), measured by rotating **H** as a function of ϕ within the *ab* plane. Angular variation disappears in $Y(Ni_{0.95}Pt_{0.05})_2B_2C$.

electron phonon coupling coexists with the AF fluctuation [97]. We note that the topology of the nodal regions plays an important role in determining the superconducting properties, such as the vortex lattice structure, reversible magnetization, upper critical field H_{c2}, etc. For instance, the extended QPs appear to be very important for the vortex triangular–square lattice phase transition [71, 98, 99].

6.2. Heavy fermion UPd_2Al_3

UPd_2Al_3 has aroused great interest among heavy fermion (HF) superconductors because of its unique properties. In UPd_2Al_3, superconductivity with heavy mass occurs at $T_c = 2.0$ K after antiferromagnetic (AF) ordering with atomic size local moments ($\mu = 0.85\ \mu_B$) sets in at $T_N = 14.3$ K [100]. Below T_c, superconductivity coexists with magnetic ordering. The ordered moments are coupled ferromagnetically in the basal hexagonal *ab* plane and line up along the *a* axis (figure 9). These ferromagnetic sheets are stacked antiferromagnetically along the *c* axis with the wavevector $\mathbf{Q_0} = (0, 0, \pi/c)$, where *c* is the *c* axis lattice constant [101]. For the structure of the hexagonal basal plane; see the inset of figure 10. The presence of large local moments is in contrast to other HF superconductors, in which static magnetic moments are either absent or very small at the onset of superconductivity [6]. Since both superconductivity and AF ordering in UPd_2Al_3 involve the Uranium 5f electrons, this system is an example of the dual nature, partly localized and partly itinerant, of strongly correlated electrons [6, 102, 103].

In the superconducting state of UPd_2Al_3, two noticeable features have been reported. The first is the 'strong coupling anomalies' observed in the tunnel junctions UPd_2Al_3–AlO_x–Pb [104] and inelastic neutron scattering, which were attributed to the strong interaction between the heavy fermion quasiparticles and AF spin wave excitations [103, 105–107]. The second feature is the appearance of a 'resonance peak' in the inelastic neutron scattering in the vicinity of $\mathbf{Q_0}$ well below T_c. Similar peak in the cuprates was interpreted as the result of the feedback effect of the opening of the superconducting gap on the electron–hole damping of the spin fluctuations, and was shown to be unique to superconductors where the gap changes sign under the translation by the AFM wavevector [108]. The analogous effect in UPd_2Al_3, which has static AFM order, rather than fluctuations, was investigated by Bernhoeft *et al* [105, 106],

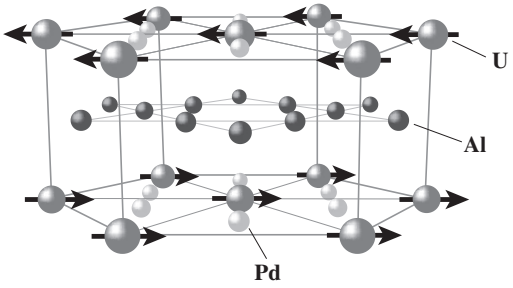

Figure 9. Crystal structure of UPd_2Al_3. AF ordering with atomic size local moments ($\mu = 0.85\ \mu_B$) sets in at $T_N = 14.3$ K. The ordered moments are coupled ferromagnetically in the basal hexagonal ab plane and line up along the a axis. These ferromagnetic sheets are stacked antiferromagnetically along the c axis.

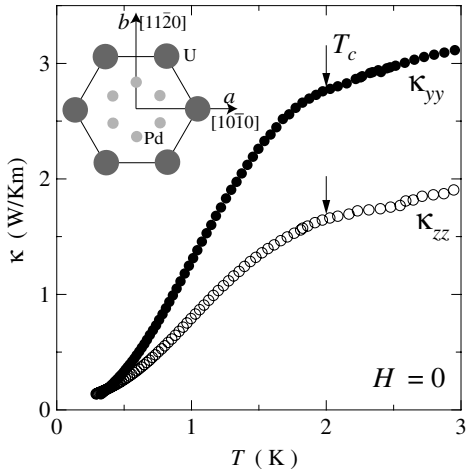

Figure 10. Temperature dependence of the thermal conductivity along the b axis κ_{yy} ($\mathbf{q} \parallel b$) and c axis κ_{zz} ($\mathbf{q} \parallel c$) in zero field. Inset: structure of the hexagonal basal plane of UPd_2Al_3 with the alignment of the a axis (100) and b axis $(-1, 2, 0)$, as used in the text.

and strongly suggests that the gap in this material changes sign under translation $\mathbf{k} \rightarrow \mathbf{k} + \mathbf{Q_0}$. The NMR Knight shift measurements indicate the spin singlet pairing, and the spin–lattice relaxation rate does not show the coherence peak at T_c, and decreases as $T_1^{-1} \propto T^3$, indicating the presence of line nodes [109]. These results provide rigorous constraints on the shape of the gap.

According to band calculations and de Haas–van Alphen measurements in the AF phase, the largest Fermi sheet with heavy electron mass and the strongest 5f admixture has the shape of a corrugated cylinder with a hexagonal in-plane anisotropy [102]. Below we assume that this cylindrical Fermi sheet with heavy mass is responsible for the superconductivity, and carry out the analysis within this model.

We measured the thermal conductivity along the c axis of the hexagonal crystal structure, κ_{zz} (heat current $\mathbf{q} \parallel c$) and along the b axis κ_{yy} ($\boldsymbol{q} \parallel b$) in high quality single crystals of UPd_2Al_3 with $T_c = 2.0$ K. (The residual resistivity ratio was 55 along the b axis and 40 along the c axis.) Figure 10 depicts the temperature dependence of κ_{yy} and κ_{zz} in zero field. Since spin wave spectrum has a finite gap of $\sim$1.5 meV at the zone centre, its contribution appears

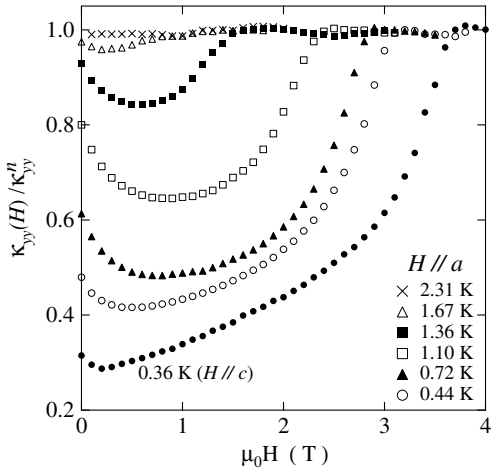

Figure 11. Field dependence of the b axis thermal conductivity κ_{yy} normalized to the normal state value just above the upper critical field, κ^n_{yy}, for $\mathbf{H} \parallel a$ and $\mathbf{H} \parallel c$.

to be negligible below T_c [109, 110]. The Wiedemann–Franz ratio $L = \frac{\kappa}{T}\rho$ at T_c is $0.95L_0$ for κ_{zz} and is $1.16L_0$ for κ_{yy}. These results indicate that the electron contribution is dominant below T_c.

Figure 11 shows the H dependence of κ_{yy} for $\mathbf{H} \parallel a$ and $\mathbf{H} \parallel c$ below T_c. For both field directions, κ_{yy} grows with H beyond an initial decrease at low fields. For $\mathbf{H} \parallel c$, κ_{yy} increases almost linearly with H, $\kappa_{yy} \propto H$, at 0.36 K. The minimum in $\kappa(H)$ is much less pronounced at lower temperatures. As H approaches $H_{c2} \parallel a$ or $\parallel b$, κ_{yy} shows a steep increase and attains its normal state value. This low to intermediate H dependence of the thermal conductivity in the superconducting state is markedly different from that observed in ordinary s wave superconductors. At high temperatures and low fields, where the condition $\sqrt{H/H_{c2}} < T/T_c$ is satisfied, the thermally excited quasiparticles dominate over the Doppler shifted quasiparticles. It has been shown that in this regime, while the Doppler shift enhances the DOS, it also leads to a concomitant reduction in both the impurity scattering time and Andreev scattering time off the vortices [45, 50, 61, 65, 111]. When this lifetime suppression exceeds the enhancement in $N(E)$, which may happen at intermediate temperatures and low fields, the non-monotonic field dependence of the thermal conductivity is found. As in other superconductors with nodes, the region of the initial decrease of the thermal conductivity shrinks at low T. Thus the H dependence of κ_{yy} in UPd_2Al_3, initial decrease at low field at high temperatures and linear behaviour $\kappa_{yy} \propto H$ at low temperatures, are in qualitative agreement with the existence of line nodes in $\Delta(\mathbf{H})$ [82, 112].

We first test whether there exist vertical line nodes perpendicular to the basal plane. Figure 12 shows $\kappa_{zz}(\mathbf{H}, \phi)$ as a function of ϕ at 0.4 K, measured by rotating $\mathbf{H}$ within the basal plane ($\theta = 90°$). Above 0.5 T, a distinct sixfold oscillation is observed in $\kappa_{zz}(\mathbf{H}, \phi)$, reflecting the hexagonal symmetry of the crystal. Sixfold oscillation is observable even above H_{c2}. On the other hand, no discernible sixfold oscillation was observed below 0.5 T within our experimental resolution. We infer that the AF magnetic domain structure and anisotropy of H_{c2} within the plane are responsible for the sixfold symmetry and the nodal structure is not related to the oscillation. According to the neutron diffraction experiments, the magnetic domain structure changes at $H_D \sim 0.6$ T well below T_N. Below H_D, the ordered moments point along the a axis forming domains, and the spin structure is not affected by the $\mathbf{H}$ rotation

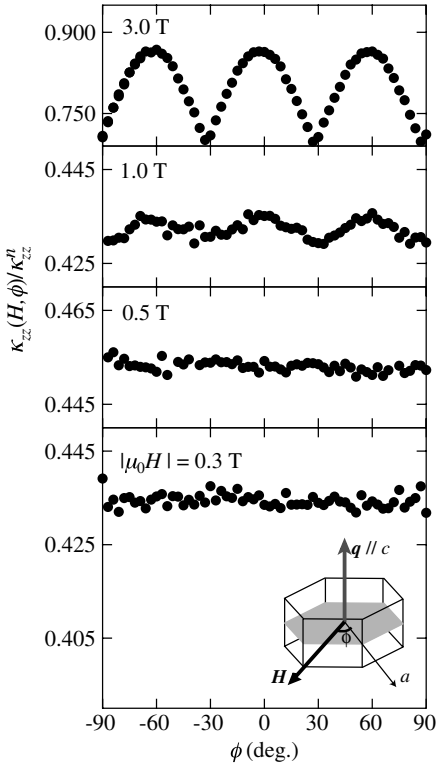

Figure 12. Angular variation of the c axis thermal conductivity $\kappa_{zz}(\mathbf{H}, \phi)$ normalized by the normal state value, κ^n_{zz}, at several fields at 0.4 K, below H_{c2} (=3.5 T). **H** was rotated within the basal plane as a function of ϕ (see the inset). A distinct sixfold oscillation is observed above 0.5 T, while oscillation is absent at 0.5 and 0.3 T.

in the basal plane. On the other hand, above H_D, the **H** rotation causes domain reorientation. Then the magnetic domain structure changes with sixfold symmetry with **H** rotation. Thus the sixfold symmetry observed in κ_{zz} above 0.5 T is most likely to be due to the magnetic domain structure. This indicates that *there are no nodes located perpendicular to the basal plane, i.e. the gap function in the basal plane is isotropic.*

We next test for the existence of the horizontal line nodes parallel to the basal plane. Figure 13 displays the angular variation of $\kappa_{yy}(\mathbf{H}, \theta)$ for rotating **H** as a function of θ within the ac plane at 0.4 K. A distinct oscillation with twofold symmetry was observed in the superconducting state. In contrast to κ_{zz}, no discernible twofold oscillation was found in the normal state above H_{c2}. We decompose $\kappa_{yy}(\mathbf{H}, \theta)$ as

$$\kappa_{yy} = \kappa^0_{yy} + \kappa^{2\theta}_{yy}, \tag{13}$$

where κ^0_{yy} is a θ independent term and $\kappa^{2\theta}_{yy} = C^{2\theta}_{yy} \cos 2\theta$ is a term with the twofold symmetry with respect to θ rotation. The field dependence of $C^{2\theta}_{yy}$ at 0.4 K is shown in figure 14(a). For comparison, the H dependence of κ_{yy} for $\mathbf{H} \parallel c$ at $T = 0.36$ K is plotted in figure 14(b). There are three regions denoted (I), (II) and (III), below H_{c2}. In the vicinity of H_{c2} ((III) region), where κ_{yy} increases steeply with H, the sign of $C^{2\theta}_{yy}$ is negative and the amplitude $|C^{2\theta}_{yy}|/\kappa^n_{yy}$ is of the order of 10%. Here κ^n_{yy} is κ_{yy} in the normal state just above H_{c2}. With decreasing H, $C^{2\theta}_{yy}$ changes sign at about 2.3 T and becomes positive in the region where κ_{yy} for $\mathbf{H} \parallel c$ shows

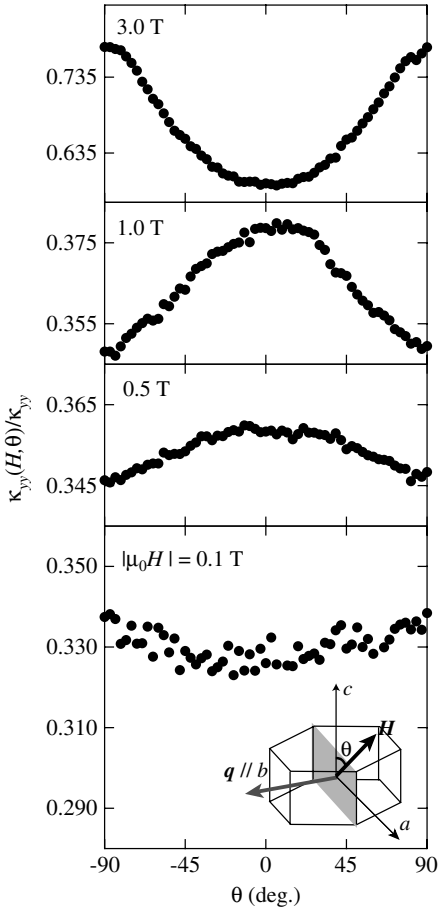

Figure 13. Angular variation of the b axis thermal conductivity $\kappa_{yy}(\mathbf{H}, \theta)$ normalized by the normal state value κ^n_{yy} at several fields at 0.4 K. **H** was rotated within the ac plane perpendicular to the basal plane (see the inset).

a linear H dependence ((II) region). Below about 0.25 T, where the second sign change takes place, κ_{yy} decreases with H ((I) region). In this region, $C^{2\theta}_{yy}$ is, once again, negative.

We address the origin of the observed twofold oscillation. The disappearance of the oscillation above H_{c2}, together with the fact that there is only one magnetic phase in this configuration [101], completely rule out the possibility that the origin is due to the magnetic domain structure. There are two possible origins for the oscillation; the nodal structure and the anisotropy of the Fermi velocity and H_{c2}. Obviously, as discussed previously, a large twofold oscillation with negative sign observed in the (III) region arises from the anisotropies of the Fermi velocity and H_{c2}. This immediately indicates that *the twofold symmetry with positive sign in the (II) region originates not from these anisotropies but from the quasiparticle structure associated with the nodal gap function.* In addition, the amplitude of $C^{2\theta}_{yy}/\kappa_{yy}$ in the (II) region is a few per cent, which is quantitatively consistent with the prediction based on the Doppler shifted DOS. We also note that the second sign change at low fields in the (I) region is compatible with the nodal structure. In this region, as discussed previously, the H dependence of the thermal conductivity is governed by the suppression of the quasiparticle scattering rate.

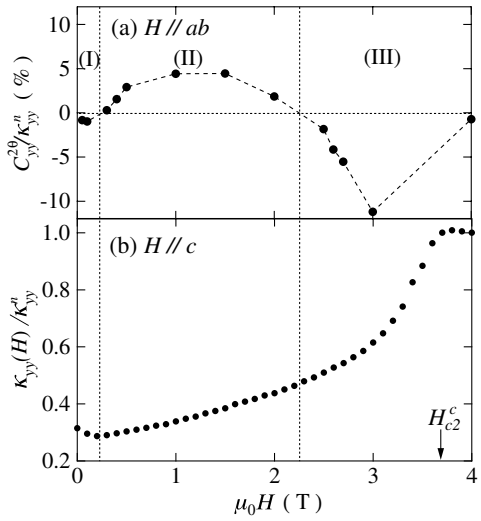

Figure 14. (a) Field dependence of the amplitude of the twofold symmetry $C_{yy}^{2\theta}$ normalized by the normal state thermal conductivity κ_{yy}^{n} at 0.4 K. (b) Field dependence of the b axis thermal conductivity κ_{yy} for $\mathbf{H} \parallel c$ at 0.36 K. The sign of $C_{yy}^{2\theta}$ is negative in the (III) region just below H_{c2} and in the (I) region where κ_{yy} decreases with H. On the other hand, the sign of $C_{yy}^{2\theta}$ is positive in the (II) region.

As discussed in [44, 58, 59, 61, 64, 111], the anisotropic carrier scattering time associated with the nodal structure also gives rise to the variation of $\kappa_{yy}(\mathbf{H}, \theta)$ as a function of θ. In this case the sign of the oscillation is opposite to that arising from the Doppler shifted DOS in the (II) region. These considerations lead us to conclude that UPd_2Al_3 has horizontal nodes. In addition, the fact that there is a single maximum structure in the angular variation of $\kappa_{yy}(\mathbf{H}, \theta)$ indicates that horizontal line nodes are located at positions where the condition $\mathbf{p} \parallel ab$ in the Brillouin zone is satisfied. Thus *the allowed positions of the horizontal nodes are restricted at the bottleneck and AF zone boundary* [62, 82].

For comparison, the angular variations of κ_{yy} and κ_{zz} at low fields are shown in figure 15. While the amplitude of the twofold oscillation $C_{yy}^{2\theta}/\kappa_{yy}$ is 3%, which is quantitatively consistent with the Doppler shifted DOS, the amplitude of the sixfold oscillation $C_{zz}^{6\theta}/\kappa_{zz}$ is less than 0.2%, which is more than 10 times smaller than the amplitude expected from the Doppler shifted DOS in the presence of nodes. Combining the results, we arrive at the conclusion that *the gap function is isotropic in the basal plane and has horizontal node.*

To discuss the position of the horizontal line node in $UPd2Al_3$, we consider a 'magnetic' Brillouin zone in a cylindrical Fermi surface, as shown in figure 16(a). The density of states is anisotropic under the rotation of the field in the ac plane, by varying the angle θ in the inset. To illustrate the difference between the line nodes at high symmetry positions in the magnetic Brillouin zone, and away from those, we consider here four model gap functions

(i) Type I: a horizontal node located at the bottleneck; $\Delta(\mathbf{k}) \propto \sin k_z c$.
(ii) Type II: a horizontal node located at the zone boundary; $\Delta(\mathbf{k}) \propto \cos k_z c$.
(iii) Type III: a hybrid of type I and II. Two horizontal nodes located at the bottleneck and the zone boundary; $\Delta(\mathbf{k}) \propto \sin 2k_z c$.
(iv) Type IV: two horizontal nodes located at positions shifted off the bottleneck in the Brillouin zone; $\Delta(\mathbf{k}) \propto \cos 2k_z c$.

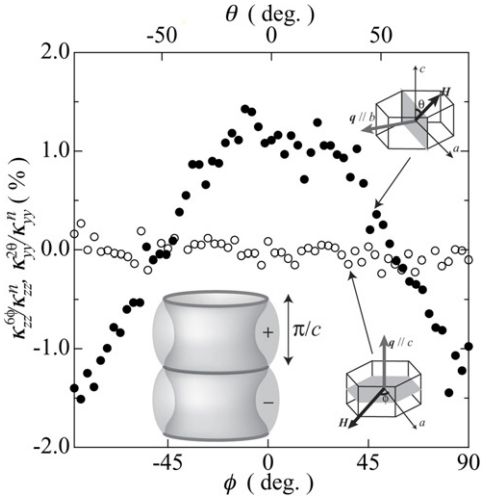

Figure 15. Angular variation of the b axis thermal conductivity $\kappa_{yy}^{2\theta}/\kappa_{yy}^{n}$ with rotating **H** within the ac plane (solid circles) and of the c axis thermal conductivity $\kappa_{zz}^{6\phi}/\kappa_{zz}^{n}$ with rotating **H** within the basal ab plane (open circles) at $T = 0.4$ K and at $H = 0.5$ T. The amplitude of the sixfold oscillation in $\kappa_{zz}^{6\phi}/\kappa_{zz}^{n}$ is less than 0.2% if it exists. Inset: schematic diagram of the gap function of UPd_2Al_3 determined by angle resolved magnetothermal transport measurements. The thick solid lines indicate horizontal nodes located at the AF zone boundaries.

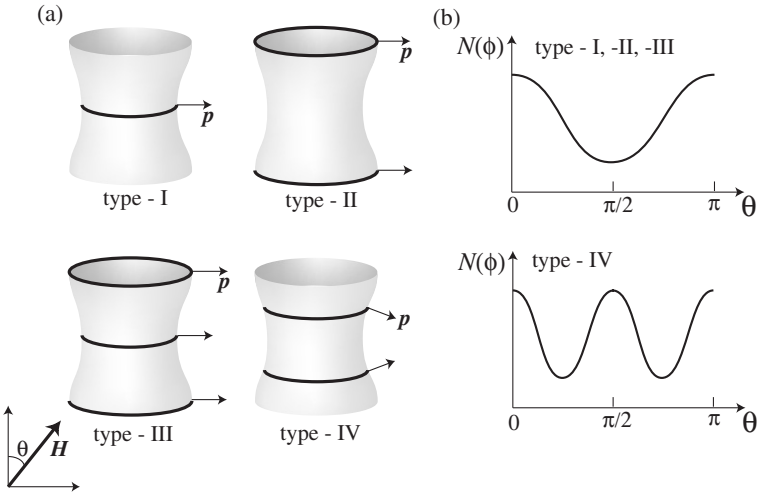

Figure 16. (a) Schematic diagram of the gap structure with horizontal line node in the magnetic Brillouin zone. Line nodes are located at the bottleneck (type I) and at the zone boundary (type II). Two line nodes are located at the bottleneck and the zone boundary (type III) and at positions shifted off the bottleneck (type IV). (b) Oscillations of the DOS for **H** rotating in the ac plane for various gap functions. Twofold oscillations with the same sign are expected for types I, II, and III. On the other hand, for type IV, an oscillation with a double minimum is expected.

The expected angular variation of the Doppler shifted DOS is a function of the relative angle between **H** and **p** for these gap functions are shown schematically in figure 16(b). The twofold oscillations with the same phase are expected for type I, II, and III gap functions,

in which the horizontal nodes are located at the position where $\mathbf{p} \parallel ab$ plane; one cannot distinguish these three gap functions when the Fermi surface has an open orbit along the c axis. For type IV, one expects an oscillation with a double minimum structure as a function of θ.

Thus, the order parameters allowed, by thermal conductivity measurements, are

(i) $\Delta(\mathbf{k}) = \Delta_0 \sin k_z c$,
(ii) $\Delta(\mathbf{k}) = \Delta_0 \sin 2k_z c$ and
(iii) $\Delta(\mathbf{k}) = \Delta_0 \cos k_z c$

which are shown in the type I, II and III gap structures in figure 16(a). Generally the first and the second represent spin triplet gap functions, and only the third, which is a spin singlet, remains a viable possibility. Note, however, that the thermal conductivity is only sensitive to the *amplitude* of the gap. Among the possible order parameters for the D_{6h} symmetry group is that transforming according to Γ_5 representation, with a basis function $k_z(k_x + ik_y)$ [1]. In that case the gap function may vary as $(k_x + ik_y) \sin k_z c$, and the gap amplitude, over a quasi-two dimensional Fermi surface, may have only weak modulations apart from the horizontal line of nodes. Such an order parameter breaks the time reversal symmetry, and we are not aware of any evidence in support of that in UPd_2Al_3; however, targeted search for a time reversal symmetry broken state in this system has not been performed. Both the first and the third gap functions are compatible with the constraint implied by the neutron resonance peak, $\Delta(\mathbf{k}) = -\Delta(\mathbf{k} + \mathbf{Q_0})$. These considerations lead us to conclude that *the gap function of* UPd_2Al_3 *is most likely to be* $\Delta(\mathbf{k}) = \Delta_0 \cos k_z c$, shown in the inset of figure 15, although we cannot exclude the possibility of the state with broken time reversal symmetry on the basis of out measurements.

For the $\cos k_z c$ pairing, the horizontal node located at the AF zone boundary indicates that pair partners cannot reside in the same basal plane. The interlayer pairing appears to indicate that strong dispersion of the magnetic excitation along k_z causes the pairing, as suggested in the magnetic exciton mediated superconductivity model [6, 103, 113]. The isotropic gap function in the basal plane implies that the pairing interaction in the neighbouring planes strongly dominates over the interaction in the same plane. Although the pairing interaction inferred from the determined gap function should be further scrutinized, the recent results imply that the interlayer pairing interaction associated with the AF interaction is most likely to be the origin of the unconventional superconductivity in UPd_2Al_3.

6.3. Skutterudite $PrOs_4Sb_{12}$

Recently discovered heavy fermion superconductor $PrOs_4Sb_{12}$ ($T_c = 1.82$ K) with filled skutterudite structure (figure 17) is relatively unique as the f electrons have a non-magnetic ground state, determined by the crystalline electric field (most probably singlet Γ_1 state) [114, 115]. The HF behaviour ($m* \sim 50m_e$, m_e is the free electron mass) is probably due to the interaction of the electric quadrupole moments of Pr^{3+} (rather than local magnetic moments as in the other HF superconductors) with the conduction electrons. Therefore the relation between the superconductivity and the orbital (quadrupole) fluctuations of f electron state excited great interest: $PrOs_4Sb_{12}$ has been proposed as a candidate for the first superconductor with pairing mediated neither by electron–phonon nor magnetic interactions, but by quadrupolar fluctuations. Even if these fluctuations do not provide the pairing glue by themselves, but only in conjunction with phonons, they have the potential for influencing the symmetry of the superconducting order parameter, which makes it of the utmost importance to determine the symmetry of the SC gap.

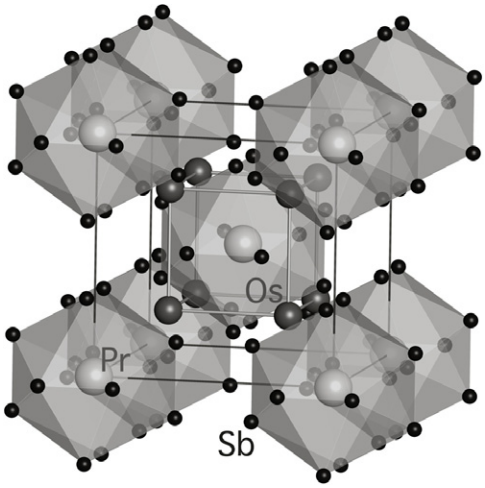

Figure 17. Crystal structure of $PrOs_4Sb_{14}$.

The unconventional superconductivity in $PrOs_4Sb_{12}$ has been suggested by several experiments. NQR measurements showed the absence of Hebel–Slichter peak [116]. In addition, the Knight shift does not change below T_c, implying that the gap function has odd parity [22]. Moreover, μSR experiments report the appearance of the static spontaneous magnetic field below T_c, which can be interpreted as the spontaneous breaking of the time reversal symmetry [33]. The penetration depth and NMR T_1^{-1} measurements indicate the presence of point nodes [117].

Figure 18 shows the T dependence of the c axis thermal conductivity κ_{zz} (the heat current $\mathbf{q} \parallel c$) divided by T both at zero field and above H_{c2} ($\simeq$2.2 T at $T = 0$ K) of $PrOs_4Sb_{12}$ single crystal (#1). In this temperature region, the electronic contribution to κ_{zz} dominates the phonon contribution. The inset of figure 18 shows the field dependence of κ_{zz} of sample #2 at very low temperature. κ_{zz} increases very steeply even at very low field ($H < 0.1$ T). When contrasted with the exponentially slow increase of the thermal conductivity with field observed in s wave superconductors at $H \ll H_{c2}$ [118], this is a strong indication that the thermal transport is governed by the delocalized QPs arising from the gap nodes. Above 0.1 T κ_{zz} increases gradually, then shows a steep increase above 0.5 T up to H_{c2}.

Figures 19(a) and (b) display the angular variation of $\kappa_{zz}(\mathbf{H}, \phi)$ in $\mathbf{H}$ rotated within the ab plane ($\theta = 90°$) at $T = 0.52$ K [68]. The measurements have been done in rotating $\mathbf{H}$ after field cooling at $\phi = -90°$. The open circles show κ_{zz} $(\mathbf{H}, \phi)$ at $H = 1.2$ and 0.5 T which are obtained under field cooling at each angle. Above H_{c2} ($\simeq$2.0 T at 0.5 K) $\kappa_{zz}(\mathbf{H}, \phi)$ is essentially independent of ϕ. A clear fourfold variation is observed just below H_{c2} down to $H \sim 0.8$ T. However further reduction of H below 0.8 T causes a rapid decrease of the amplitude of the fourfold term, and its disappearance below 0.7 T. At the same time, the twofold component grows rapidly. This surprising behaviour suggests a change in the gap symmetry as a function of field in the superconducting state.

Figure 20 shows the H dependence of the amplitudes of the twofold and the fourfold terms, which are obtained by decomposing $\kappa_{zz}(\mathbf{H}, \phi)$ as

$$\kappa_{zz}(\mathbf{H}, \phi) = \kappa_{zz}^0 + \kappa_{zz}^{2\phi} + \kappa_{zz}^{4\phi}, \tag{14}$$

where κ_{zz}^0 is a ϕ independent term, $\kappa_{zz}^{2\phi} = C_{2\phi} \cos 2\phi$, and $\kappa_{zz}^{4\phi} = C_{4\phi} \cos 4\phi$ are the terms with twofold and fourfold symmetry with respect to ϕ rotation. It is clear that the transition from

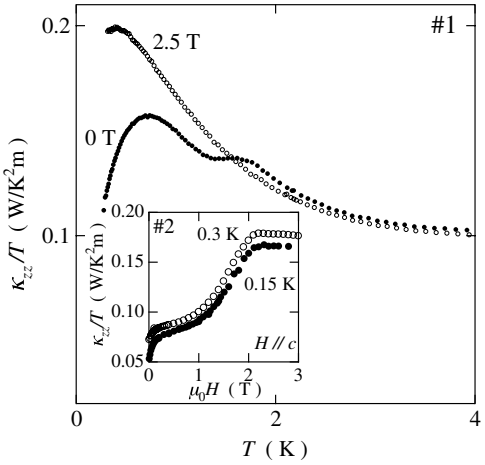

Figure 18. Temperature dependence of the c axis thermal conductivity κ_{zz} (the heat current $\mathbf{q} \parallel c$) divided by T at zero field (solid circles) and at 2.5 T (open circles) above H_{c2} ($\simeq$2.2 T at $T = 0$ K) of $PrOs_4Sb_{12}$ single crystal (#1). Inset: field dependence of κ_{zz}/T of sample #2 at very low temperature.

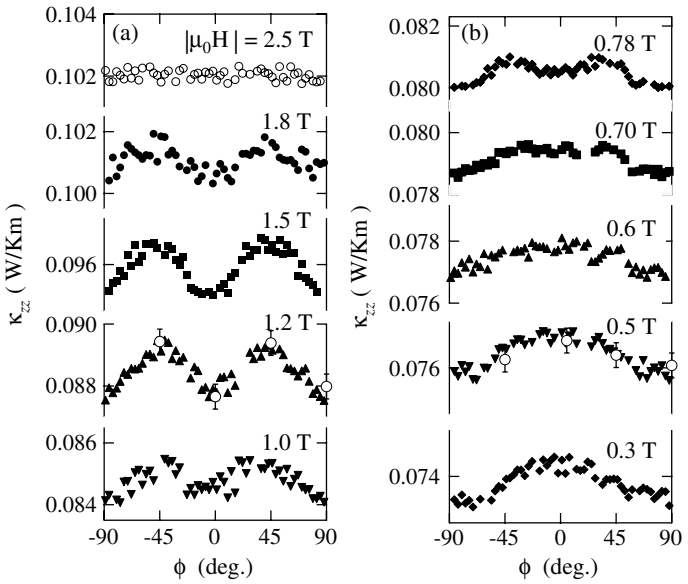

Figure 19. ((a), (b)) Angular variation of κ_{zz} ($\mathbf{q} \parallel c$) in $\mathbf{H}$ rotating within the ab plane as a function of ϕ at 0.52 K above and below H_{c2} ($\simeq$2.0 T).

the fourfold to twofold symmetry in ϕ rotation is sharp, and occurs in a narrow field range at $H/H_{c2} \simeq 0.4$, deep inside the SC phase. Both symmetries coexist in a narrow field range. If the minima of the thermal conductivity are associated with the direction of the field along the nodes, the reduced $\kappa_{zz}(\mathbf{H}, \phi)$ at $\phi = \pm 90°$ and $0°$ in the high field phase, and at $\phi = \pm 90°$ for the low field phase, respectively, lead to the conclusion that the nodes are along the [100] and [010] directions in the high field phase, while they are located only along the [010] direction in the low field phase.

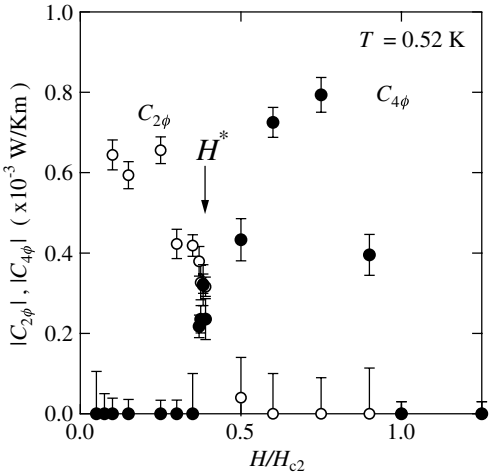

Figure 20. The amplitude of twofold (open circles) and fourfold (filled circles) symmetries, $|C_{2\phi}|$ and $|C_{4\phi}|$, respectively, plotted as a function of H/H_{c2} at $T = 0.52$ K. At H^*, the crossover from twofold to fourfold symmetry takes place.

Having established the presence of nodes, the next question is their classification. As discussed in section 4.1, the angular variation of κ_{zz} can distinguish between the point and line nodes, by rotating **H** conically around the c axis with a tilted angle from the ab plane. Although we do not show it here, the amplitude at $\theta = 45°$ and 30° is smaller than that at $\theta = 90°$ [68]. Similar results were obtained for the twofold symmetry.

What is the nodal structure inferred from the present results? The ϕ rotation of the field can only provide the information of the nodes away from the [001] direction. We shall therefore appeal to the group theoretical consideration for the discussion of the nodal structure. It is unlikely that the SC gap function has only four point nodes in the cubic T_h crystal symmetry: this is independent of the spin singlet or triplet symmetry. Hence the likely scenario is that the gap function at high field phase has six point nodes. The low field phase is likely to have two nodes, although on the basis of the experimental observations we cannot exclude the four node structure (along [001] and [010]).

The H–T phase diagram of the SC symmetry determined by the present experiments is displayed in figure 21. The filled circles represent the magnetic field H^* at which the transition from fourfold to twofold symmetry takes place. The H^* line which separates two SC phases (high field A phase and low field B phase) lies deep inside the SC state. We note that recent flux flow resistivity measurements also reported an anomaly at H^*. The only example of a superconductor with multiple phases of different gap symmetry so far has been UPt_3 [119]. In that case the degenerate transition temperatures for the two orders at zero field can be split by, for example, applying pressure. Therefore it is important to determine (a) whether the two phases manifested in the thermal conductivity measurements have the same T_c in zero field; (b) whether the transition can be split by influencing the system by an experimental handle other than the field. It seems logical that, if the gap structure suggested here is indeed realized, application of the uniaxial pressure along the [100] direction should lift the symmetry of the gap and favour one of the two phases.

Recently, small angle neutron scattering experiments reported the hexagonal flux line lattice, which is distorted with a twofold symmetry [120]. It has been pointed out that the distortion originates from the nodal gap structure, which provides a strong support of the

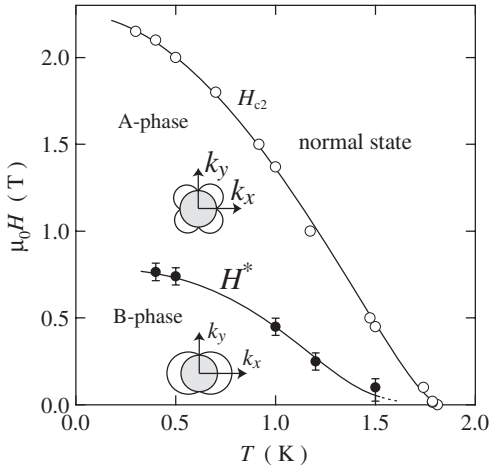

Figure 21. The phase diagram of the superconducting gap symmetry determined by the present experiments. The filled circles represent the magnetic field H^* at which the transition from fourfold to twofold symmetry takes place. The open circles represent H_{c2}. The area of the gap function with fourfold symmetry is shown as A phase and the area of the gap function with twofold symmetry is shown as B phase.

present angular variation of $\kappa_{zz}(\mathbf{H}, \phi)$. We also note that the possible existence of the third phase was predicted by the magnetization and penetration depth measurements [117, 121].

Thus $PrOs_4Sb_{12}$ has several unique features. In almost all superconducting (SC) materials known to date, once the energy gap in the spectrum of electrons opens at the SC transition, only its overall amplitude, and not the shape and symmetry around the Fermi surface, changes in the SC phase [122]. In contrast, $PrOs_4Sb_{12}$ seems to have several superconducting phases with different symmetries. Many heavy fermion superconductors have *line* nodes in the gap functions (with possible additional point nodes). The suggestion that $PrOs_4Sb_{12}$ is the first heavy fermion superconductor, in which only the point nodes are identified may be the key for understanding the superconductivity mechanism due to quadrupolar interaction.

7. Quasi-two dimensional superconductors

We now discuss the implications of the thermal conductivity measurements for the nodal structure of three superconductors, $CeCoIn_5$, κ-$(BEDT\text{-}TTF)_2Cu(NCS)_2$, and Sr_2RuO_4. These materials look very different at first sight but reveal several similar features. First, all three have strong electron–electron correlations. Second, they all have quasi-two dimensional electronic structure, as confirmed by the band structure calculation and by the dHvA measurements. This is also supported by a relatively large anisotropy of the upper critical field between inequivalent crystalline directions. Third, the power laws in the temperature dependence of thermodynamic quantities in the superconducting state is consistent with the presence of line nodes in the superconducting gap. The position of the line nodes is still an open question in many of these materials, and is the focus of our analysis here.

Unfortunately, in all these compounds, the out-of-plane thermal conductivity is difficult to measure due to thin plate-like single crystal samples. We therefore measured the in-plane thermal conductivity with magnetic field rotated within the same conducting plane. In this geometry, the dominant signal is twofold symmetric, and simply depends on the angle between the thermal current, $\mathbf{q}$, and $\mathbf{H}$ due to the difference in the transport along and normal to the

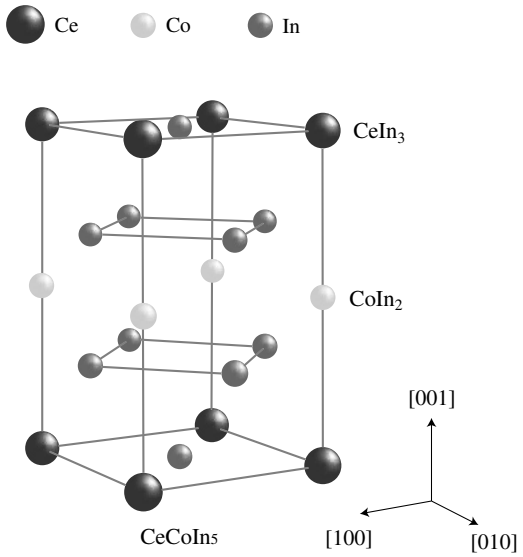

Figure 22. Crystal structure of $CeCoIn_5$.

vortices. This twofold oscillation is not directly related to the nodal structure, and the challenge for the interpretation is to separate it from the features due to the nodes.

7.1. $CeCoIn_5$

The family of the heavy fermion superconductors $CeTIn_5$ (T = Rh, Ir, and Co) was discovered in 2001 [123]. Both $CeIrIn_5$ and $CeCoIn_5$ are ambient pressure superconductors, with transition temperatures of 0.4 and 2.3 K, respectively. $CeRhIn_5$ is an antiferromagnet, but shows superconductivity under moderate pressure. The crystal structure of $CeTIn_5$ is tetragonal consisting of the conducting $CeIn_3$ layers separated by less conducting TIn_2 layers (figure 22). In the normal state $CeCoIn_5$ exhibits non-Fermi-liquid behaviour, probably related to the strong AFM fluctuations; moreover, there is evidence that superconductivity appears in the neighbourhood of a quantum critical point (QCP), possibly of AFM origin [124–127]. For that reason $CeCoIn_5$ is an excellent candidate to study the relationship between QCP and unconventional superconductivity. The temperature dependence of the heat capacity and thermal conductivity [128], thermal Hall conductivity [129], NMR relaxation rate [130] all indicate the presences of line nodes. The penetration depth measurements [131–133] in general support this conclusion although the low T exponents are anomalous. Recent Andreev reflection measurements indicate the sign change of the superconducting order parameter [134–136], see, however, [137] for comments on [135]. The Knight shift measurement of $CeCoIn_5$ indicates the even spin parity [130].

There are indications that the upper critical field in $CeCoIn_5$ is paramagnetically (Pauli) limited. At low T the phase transition at H_{c2} is first order, as revealed by a step in the H dependence of the thermal conductivity, magnetization, and specific heat [61, 138, 139]. Moreover, measurements of heat capacity [140, 141], ultrasound [142], and NMR [143] revealed a new superconducting phase at low temperatures in the vicinity of H_{c2} at low temperatures ($\mathbf{H} \parallel ab$). This new phase was conjectured to be the spatially inhomogeneous superconducting state (Fulde–Ferrell–Larkin–Ovchinnikov state), which was predicted four decades ago, not previously observed.

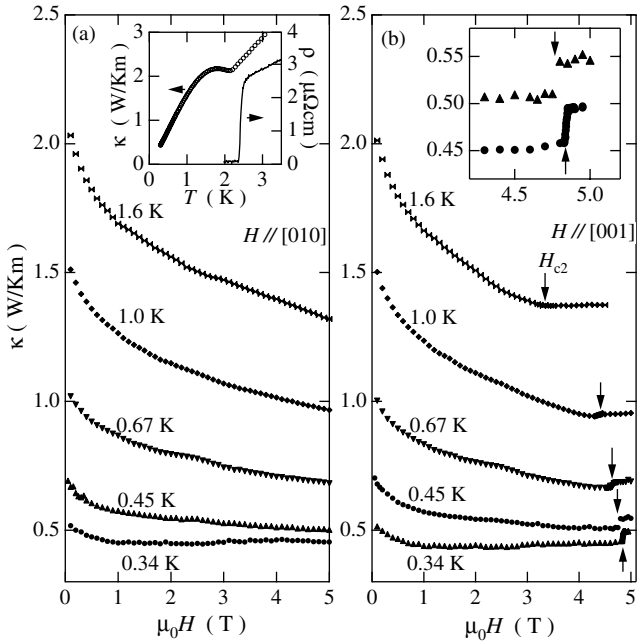

Figure 23. Field dependence of the a axis thermal conductivity (**q** ∥ [100]) for (a) **H** ∥ [001] and (b) **H** ∥ [010] below T_c. Inset of (a) κ and ρ in zero field. Inset of (b) field dependence of κ near H_{c2} at 0.45 K (○) and 0.34 K (●). The thermal conductivity jumps at H_{c2}, indicating the first order phase transition.

The inset of figure 23(a) shows the T dependence of κ and ρ. Upon entering the superconducting state, κ exhibits a sharp kink and rises to the maximum value at $T \sim 1.7$ K. The Wiedemann–Franz ratio $L = \frac{\kappa}{T}\rho \simeq 1.02L_0$ at T_c is very close to the Lorenz number $L_0 = 2.44 \times 10^{-8}\ \Omega\ \mathrm{W\ K^{-1}}$, indicating that the electronic contribution is dominant. Therefore the enhancement of κ below T_c is due to the suppression of the inelastic scattering rate, similar to the high T_c cuprates. Figures 23(a) and (b) depict H dependence of κ for **H** ∥ ab ($H_{c2} \simeq 11$ T) and **H** ⊥ ab ($H_{c2} \simeq 5$ T) below T_c, respectively. At all temperatures, κ decreases with H, and the H dependence is less pronounced at lower T in both configurations. For **H** ⊥ ab, κ has a discontinuous jump to the normal state value at H_{c2} below 1.0 K (see also the inset of figure 23(b)), indicating a first order phase transition. The data in figures 23(a) and (b), in which the H dependence of κ is more gradual with decreasing T, are consistent with the picture where the scattering of the field induced QPs is the main origin for the H dependence of κ.

Given the complexity and richness of behaviour of this superconductor, it is natural to ask whether one can draw conclusions about the symmetry of the gap from the analysis of the thermal conductivity rooted essentially in a BCS-like theory. We believe that the answer is affirmative. In the following it is important to note that all the measurements are done far below the upper critical field, i.e. far away from the possible competing states, first order transition, and quantum critical behaviour. The thermal conductivity is measured at temperatures far below that of the inelastic scattering induced peak in $\kappa(T)$. Consequently, we believe that, similar to the high T_c superconductors, the BCS-like model gives the semiquantitatively correct results in this regime.

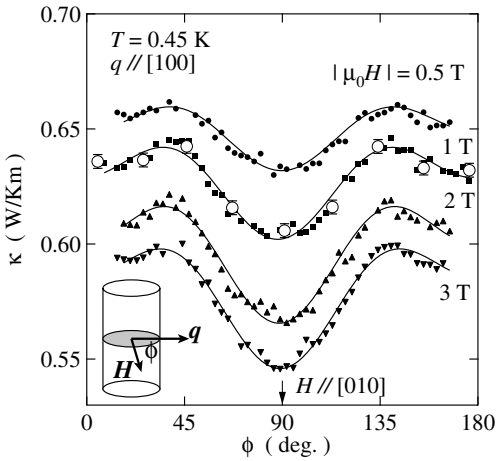

Figure 24. The a axis thermal conductivity $\kappa(H,\phi)$ ($\mathbf{q} \parallel a$) in $\mathbf{H}$ rotated within the ab plane as a function of ϕ for $CeCoIn_5$. ϕ is the angle between $\mathbf{q}$ and $\mathbf{H}$ (see the inset). The solid lines represent the result of the fitting by the function $\kappa(H,\phi) = C_0 + C_{2\phi}\cos 2\phi + C_{4\phi}\cos 4\phi$, where C_0, $C_{2\phi}$ and $C_{4\phi}$ are constants. The solid circles represent $\kappa(H,\phi)$ at $H = 1$ T which are obtained under the field cooling condition at every angle.

Figure 24 displays $\kappa(H,\phi)$ as a function of $\phi = (\mathbf{q},\mathbf{H})$ at $T = 0.45$ K of $CeCoIn_5$ [61]. The solid circles in figure 24 show $\kappa(H,\phi)$ at $H = 1$ T which are obtained under the field cooling at each angle. In all data, as shown by the solid lines in figure 2, $\kappa(H,\phi)$ can be decomposed into three terms,

$$\kappa(\phi) = \kappa_0 + \kappa_{2\phi} + \kappa_{4\phi}, \tag{15}$$

where κ_0 is a ϕ independent term, and $\kappa_{2\phi} = C_{2\phi}\cos 2\phi$ and $\kappa_{4\phi} = C_{4\phi}\cos 4\phi$ are terms with twofold and fourfold symmetry with respect to the in-plane rotation, respectively.

Figures 25(a)–(d) display $\kappa_{4\phi}$ (normalized by the normal state value κ_n). It is clear that $\kappa_{4\phi}$ exhibits a maximum at $\mathbf{H} \parallel [110]$ and $[1\bar{1}0]$ at all temperatures. Figure 4 and the inset show the T and H dependences of $|C_{4\phi}|/\kappa_n$. Below T_c the amplitude of $\kappa_{4\phi}$ increases gradually and shows a steep increase below 1 K with decreasing T. At low temperatures, $|C_{4\phi}|/\kappa_n$ becomes greater than 2%.

We note that the anisotropy of H_{c2} ($H_{c2}^{\parallel[100]} \simeq 1.03 H_{c2}^{\parallel[110]}$) is too small to explain the large amplitude of $|C_{4\phi}|/\kappa_n > 2\%$ at $H \ll H_{c2}$. Further, and more importantly, the sign of the observed fourfold symmetry is opposite to the one expected from the anisotropy of H_{c2}. The observed fourfold symmetry above T_c is extremely small; $|C_{4\phi}|/\kappa_n < 0.2\%$. Thus the anisotropies arising from H_{c2} and the band structure are incompatible with the data. Note also that, even if there is a fraction of electrons that remain uncondensed at low T, as was recently suggested [144], they can only influence the twofold (via the orbital magnetoresistance), rather than the fourfold symmetry. These considerations lead us to conclude that *the fourfold symmetry with large amplitude well below T_c originates from the QP structure.*

We now address the sign of the fourfold symmetry. For nodal lines perpendicular to the layers, two effects compete in determining $\kappa_{4\phi}$. The first is the DOS oscillation under the rotation of $\mathbf{H}$ within the ab plane. The second is the quasiparticle scattering off the vortex lattice, which has the same symmetry as the gap function [50, 53, 58, 59]. As discussed above, it is likely that at $T \approx 0.25T_c$ and $H \leqslant 0.25H_{c2}$ the second effect is dominant [50, 53]. In this case, κ attains the maximum value when $\mathbf{H}$ is along a node and has a minimum when $\mathbf{H}$

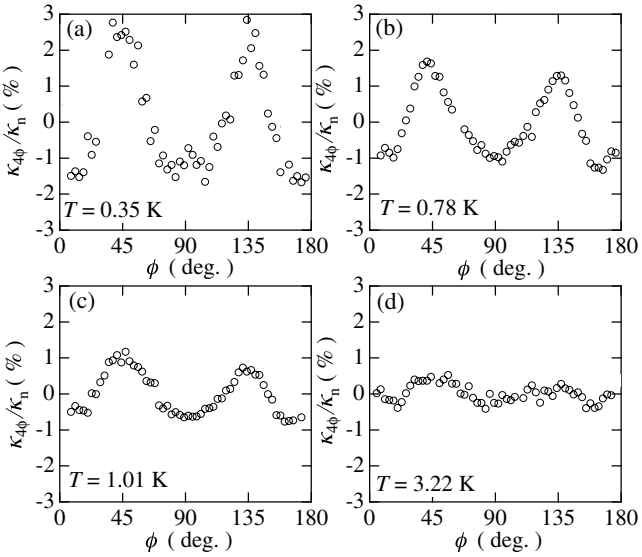

Figure 25. ((a)–(d)) The fourfold symmetry $\kappa_{4\phi}$ normalized by the normal state value κ_n at several temperatures.

is directed towards the antinodal directions [46, 53, 58, 59, 64]. The amplitude of the fourfold symmetry $|C_{4\phi}|$ in quasi-2D d wave superconductors is roughly estimated to be a few per cent of κ_n [46, 53], which is of the same order as the experimental results.

It is interesting to compare our results on $CeCoIn_5$ with the corresponding results on $YBa_2Cu_3O_{7-\delta}$, in which the fourfold symmetry has been reported in the regime where the Andreev scattering dominates. In $YBa_2Cu_3O_{7-\delta}$ with $d_{x^2-y^2}$ symmetry, $\kappa_{4\phi}$ has maxima at **H** $\parallel$ [110] and [1$\bar{1}$0] [58, 59, 64], in accord with our $CeCoIn_5$ data. Thus the sign of the present fourfold symmetry indicates *the superconducting gap with nodes located along the* $(\pm\pi, \pm\pi)$*-directions, similar to the high-*T_c *cuprates; CeCoIn*$_5$ *most probably belongs to the* $d_{x^2-y^2}$ *symmetry*.

It is worth commenting on the gap symmetry of $CeCoIn_5$ determined from the other techniques. Small angle neutron scattering experiments have reported the square lattice of flux lines [145], whose orientation relative to the crystal lattice is consistent with the expectation for the $d_{x^2-y^2}$ symmetry. Recent point contact spectroscopy, which measured the Andreev reflection at the normal metal/$CeCon_5$ interface with two crystallographic orientations, (001) and (110), have also concluded that the symmetry is $d_{x^2-y^2}$ [136]. In contrast to these results, the angular variation of the heat capacity in **H** rotated within the *ab* plane originally was interpreted as evidence for the d_{xy} symmetry [69]. However, recent theoretical analysis suggested that, when the redistribution of the spectral density due to vortex scattering is accounted for, the specific heat is also consistent with the $d_{x^2-y^2}$ gap [53].

Therefore most of the measurements suggests that this material has $d_{x^2-y^2}$ gap symmetry, probably implying that the antiferromagnetic fluctuations are important for superconductivity. This observation qualitatively agrees with recent NMR and neutron scattering experiments which reported anisotropic spin fluctuations. While $CeCoIn_5$ is a very complex system, we believe that the measurements of the field induced anisotropy provide a strong evidence for the symmetry of the superconducting gap.

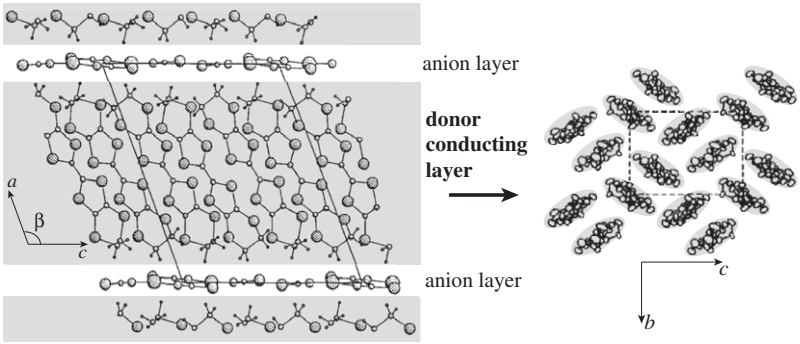

Figure 26. Crystal structure of κ-(BEDT-TTF)$_2$Cu(NCS)$_2$.

7.2. κ-(BEDT-TTF)$_2$Cu(NCS)$_2$

The nature of the superconductivity in quasi-2D κ-(BEDT-TTF)$_2$X salts (in the following abbreviated as κ-(ET)$_2$X), where the ion X can, for example, be Cu(SCN)$_2$, Cu[N(CN)$_2$]Br or I_3, has attracted considerable attention. In these compounds, the large molecules are coupled, forming narrow bands with low carrier density. It is known that ET molecules constitute a two dimensional conducting sheet in the crystal bc plane, alternating with insulating layers of anions X. Within the conducting layer, ET molecules are arranged in dimer pairs with alternating orientations (figure 26). In κ-(ET)$_2$Cu(NCS)$_2$, superconductivity occurs in proximity to the AF ordered state in the phase diagram, implying that the AF spin fluctuations should play an important role for the occurrence of superconductivity; some (but not all) of the electronic properties of these superconductors are strikingly similar to the high T_c cuprates [146, 147].

The structure of the superconducting order parameter of κ-(ET)$_2$X salts has been examined by several techniques [14]. Results strongly favouring d wave pairing with line nodes came from NMR [148, 149], thermal conductivity, and penetration depth [151, 152] experiments [150] on X = Cu[N(CN)$_2$]Br and Cu(NCS)$_2$. The STM [153] and mm-wave transmission [154] experiments reported strong modulation of the gap structure, although they arrived at very different conclusions regarding the nodal directions. In contrast to these experiments, specific heat measurements on κ-(ET)$_2$Cu[N(CN)$_2$]Br near T_c suggested a full gap [155].

Figure 27 depicts the T dependence of κ. Since the phonon thermal conductivity, κ^{ph}, dominates the electronic contribution, κ^{el}, near T_c, the enhancement of κ below T_c reflects the increase of the phonon mean free path as the electron pairs condense. Figures 28(a) and (b) depict the H dependence of κ in perpendicular ($\mathbf{H} \perp bc$ plane) and parallel ($\mathbf{H} \parallel bc$ plane) field, respectively. In the perpendicular field, $\kappa(H)$ shows a monotonic decrease up to H_{c2} above 1.6 K, which can be attributed to the suppression of the phonon mean free path by the introduction of the vortices [150, 156]. Below 1.6 K, $\kappa(H)$ exhibits a dip below H_{c2}. The minimum of $\kappa(H)$ arises from the competition between κ^{ph}, which always decreases with H, and κ^{el}, which increases steeply near H_{c2}. Consequently the magnitude of the increase of $\kappa(H)$ below H_{c2} provides a lower limit of the electronic contribution, which grows rapidly below 0.7 K; κ_n^{el}/κ_n is roughly estimated to be $\gtrsim$5% at 0.7 K and $\gtrsim$15% at 0.42 K, where κ_n^{el} and κ_n are the electronic and total thermal conductivity in the normal state above H_{c2}, respectively.

We now move on to the angular variation of κ as $\mathbf{H}$ is rotated within the 2D bc plane. Figures 29(a)–(c) display $\kappa(\mathbf{H}, \phi)$ as a function of $\phi = (\mathbf{q}, \mathbf{H})$ at low temperatures. Above

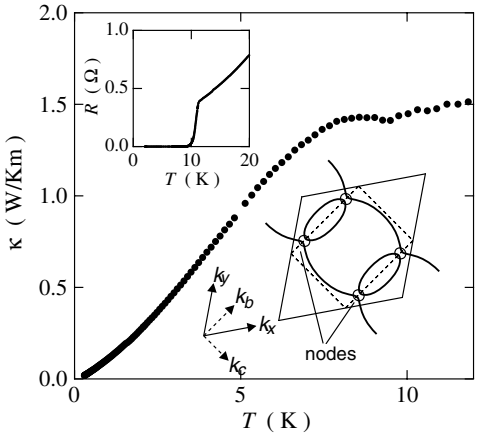

Figure 27. Temperature dependence of the thermal conductivity in zero field. The heat current **q** was applied along the b axis. Upper inset: the resistive transition at T_c. Lower inset: the Fermi surface of κ-$(ET)_2Cu(NCS)_2$. The Fermi surface consists of quasi-1D and 2D hole pocket. The node directions determined in our experiment are also shown.

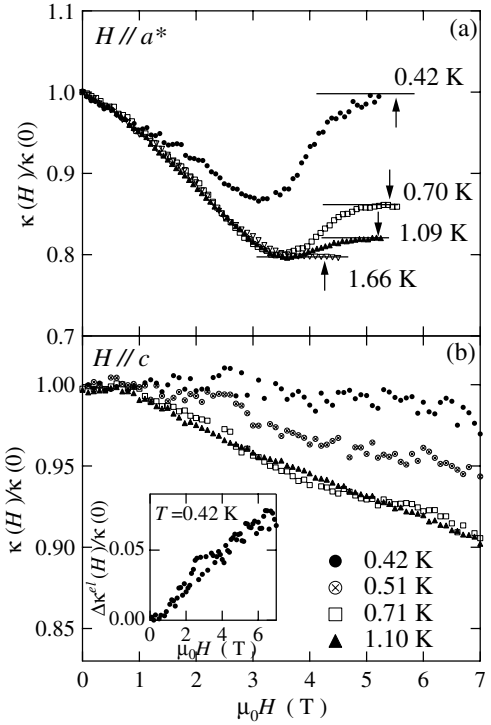

Figure 28. Field dependence of the in-plane thermal conductivity (a) in perpendicular and (b) in parallel field (**H** ∥ c) at low temperatures. Deviation from the horizontal line shown by arrows marks H_{c2}. Inset: field dependence of the electronic thermal conductivity $\Delta\kappa^{el}$ in parallel field.

0.72 K $\kappa(\mathbf{H}, \phi)$ shows a minimum at $\phi = 90°$, indicating simply that the transport is better for the heat current parallel to the vortices. On the other hand, at lower temperatures, the angular

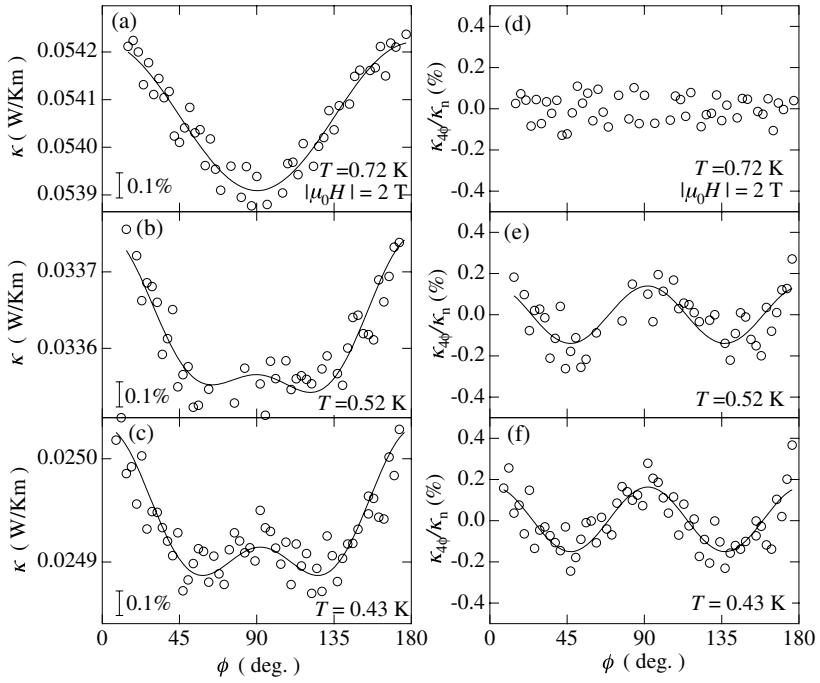

Figure 29. ((a)–(c)) Angular variation of $\kappa(\mathbf{H},\phi)$ in $|\mu_0\mathbf{H}| = 2$ T for different temperatures. ϕ is the angle between $\mathbf{q}$ and $\mathbf{H}$. The solid lines represent the result of the fitting by the function $\kappa(H,\phi) = C_0 + C_{2\phi}\cos 2\phi + C_{4\phi}\cos 4\phi$, where C_0, $C_{2\phi}$ and $C_{4\phi}$ are constants. ((d)–(f)) The fourfold symmetry $\kappa_{4\phi}$ obtained from (a) to (c).

variation changes dramatically, exhibiting a double minimum as shown in figures 29(b) and (c). In all data, we fit $\kappa(\phi)$ as a sum of three terms: a constant, a twofold, $\kappa_{2\phi}$, and a fourfold, $\kappa_{4\phi}$. These fits are shown by the solid lines in figures 29(a)–(c). Since a large twofold symmetry is observed even above 0.7 K, where $\kappa^{\rm ph}$ dominates, $\kappa_{2\phi}$ is mainly phononic in origin. In what follows, we will address the fourfold symmetry which is directly related to the electronic properties.

Figures 29(d)–(f) display $\kappa_{4\phi}$ normalized by κ_n [66]. At $T = 0.72$ K, the fourfold component is small: $|C_{4\phi}|/\kappa_n < 0.1\%$. On the other hand, a clear fourfold component with $|C_{4\phi}|/\kappa_n \sim 0.2\%$ is resolved at 0.52 and 0.43 K. As discussed before, the contribution of $\kappa^{\rm el}$ grows rapidly below 0.7 K and constitutes a substantial portion of the total κ at 0.4 K. Therefore it is natural to consider that *the fourfold oscillation is purely electronic in origin.* Although $|C_{4\phi}|$ at 0.42 K is as small as 0.2% in κ_n, it is probably close to 1.5–2% of $\kappa_n^{\rm el}$ and is also a few per cent of $\kappa^{\rm el}(0)$, assuming $\kappa_n^{\rm el}/\kappa_n \sim 0.15$. The band structure of the crystal is very unlikely to be an origin of the fourfold symmetry, as the Fermi surface of this material is nearly elliptic with twofold symmetry, and the fourfold modulation is negligible, if present at all [157]. Hence we conclude that *the observed fourfold symmetry originates from the superconducting gap nodes.*

The main question is whether the anisotropy of $\kappa^{\rm el}$ is associated with the DOS oscillation or Andreev scattering off the vortices. From general arguments [50, 53], the density of state effects dominate at low T, such as our experimental temperature of $T_c/30$. Also, since $\kappa^{\rm el}$ increases with H, as shown in the inset of figure 2(b), we believe that the DOS enhancement underlies the H dependence of $\kappa^{\rm el}$ at 0.42 K.

If the DOS oscillations indeed dominate, $\kappa^{\rm el}$ attains its maximum value when **H** is directed along the antinodal directions, and has a minimum when **H** is along the nodes. According to [53, 111], $|C_{4\phi}|$ in the d wave superconductors arising from the DOS oscillation is roughly estimated to be a few per cent of $\kappa^{\rm el}(0)$, which is in the same order to the experimental results. Since $\kappa_{4\phi}$ exhibits a maximum when **H** is applied parallel to the b and c axes of the crystal, we conclude that *the gap nodes are along the directions rotated* 45° *relative to the b and c axes*; the nodes are situated near the band gap between the 1D and 2D bands (see the upper inset of figure 1). This result is consistent with the STM experiments [153].

We emphasize that *the determined nodal structure is inconsistent with the recent theories based on the AF spin fluctuations*. In the AF spin fluctuation scenario, it is natural to expect the nodes to be along the b and c directions since the AF ordering vector is along the **b** axis, which provides partial nesting. If we take the same conventions for the magnetic Brillouin zone as in the high $T_{\rm c}$ cuprates with $d_{x^2-y^2}$ symmetry (see figure 1(c) in [147]), the superconducting gap symmetry of κ-$(ET)_2Cu(NCS)_2$ is d_{xy}. Recently, it has been suggested that the nodal structure depends on the hopping integral between ET molecules, even if the superconductivity is mediated by AF fluctuation. For instance, d_{xy} symmetry dominates over $d_{x^2-y^2}$ when the dimerization of ET molecules is not too strong, which appears to be the case for κ-$(ET)_2Cu(NCS)_2$ [158]. Moreover, when the second nearest neighbour hopping integral t_b between the dimer is comparable to the nearest neighbour hopping integral $t_{\rm c}$ ($t_b \sim t_{\rm c}$), the d_{xy} symmetry is stabilized [159]. Indeed, in κ-$(ET)_2Cu(NCS)_2$, $t_b/t_{\rm c}$ is 0.8, which is close to unity. It has also been argued that the charge fluctuations rather than spin fluctuations may be relevant to the unconventional superconductivity in κ-$(ET)_2Cu(NCS)_2$. Consequently, our results for the gap symmetry should serve as a constraint on future development of the theories of superconductivity in this family of compounds.

7.3. Sr_2RuO_4

Ever since its discovery in 1994 [8], the superconducting properties of the layered ruthenate Sr_2RuO_4 attracted considerable interest [160]. The crystal structure of this material is same as La_2CuO_4, a parent compound of high $T_{\rm c}$ cuprates (figure 30).

The superconducting state of Sr_2RuO_4 stimulated great interest because NMR Knight shift remains unchanged from the normal state value below $T_{\rm c}$, indicating that the pairing state may be a spin triplet [24]. Recent phase sensitive experiments are controversial: although odd parity of the superconducting wavefunction was suggested by [161], it was also claimed that the result of [161] can be interpreted in the even parity framework [162]. μSR measurements report the appearance of static spontaneous magnetic field below $T_{\rm c}$, which can be interpreted as a sign of broken time reversal symmetry [32]. The specific heat C_p [163], NMR relaxation rate [164] and thermal conductivity [165] indicate the presence of nodal lines in the superconducting gap. These results have motivated theorists to propose new models for the superconductivity in the ruthenates [166–169]. We, of course, address this issue here from the standpoint of the thermal conductivity measurements.

Inset of figure 31(a) shows the T dependence of κ/T in zero field for crystals with $T_{\rm c} = 1.35$ K and 1.5 K. The system is very pure, as is clear from the electrical resistivity of the order of 0.1 $\mu\Omega$ cm. At low T the electronic contribution to the thermal conductivity is dominant. At the superconducting transition, $\kappa/T(H)$ shows a kink. Figures 31(a) and (b) show the H dependence of κ for the sample with $T_{\rm c} = 1.45$ K in perpendicular (**H** $\perp$ ab plane) and parallel fields (**H** $\parallel$ ab plane), respectively. In both orientations, κ increases with H after an initial decrease at low fields. The subsequent minimum is much less pronounced at lower temperatures. At low T, κ increases linearly with H. For the in-plane field κ rises very

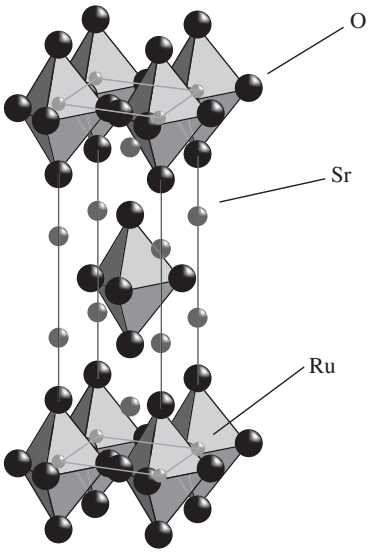

Figure 30. Crystal structure of Sr_2RuO_4.

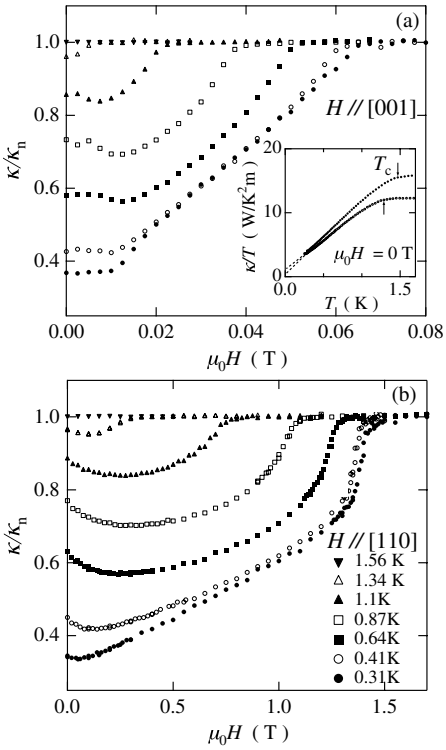

Figure 31. Field dependence of the in-plane thermal conductivity ($\mathbf{q} \parallel [110]$) of Sr_2RuO_4 ($T_c = 1.45$ K) in (a) perpendicular field $\mathbf{H} \perp ab$ plane and (b) parallel field $\mathbf{H} \parallel [110]$. In perpendicular field, κ is independent of H below the lower critical fields. Inset: temperature dependence of κ/T in zero field for two crystals with different T_c ($T_c = 1.45$ and 1.32 K).

rapidly as H approaches H_{c2} and attains its normal value with a large slope ($d\kappa/dH$), while κ in perpendicular field remains linear in H up to H_{c2}. In superconductors the slope of $\kappa(H)$ below H_{c2} increases with purity of the sample [156], so that the data for the in-plane field suggest a clean limit. A rough estimate can be done as follows: let Γ be the pair breaking parameter

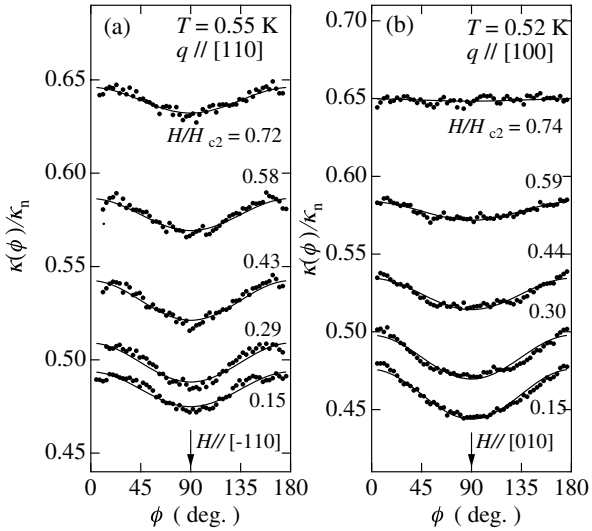

Figure 32. (a) In-plane thermal conductivity normalized by the normal state value in **H** rotated within the *ab* plane as a function of ϕ of Sr_2RuO_4 ($T_c = 1.45$ K). **q** is applied to the [110] direction. (b) The same plot for the sample with $T_c = 1.37$ K. **q** is applied to the [100] direction. ϕ is the angle between **H** and **q**. The solid lines represent the twofold component in $\kappa(\phi)/\kappa_n$.

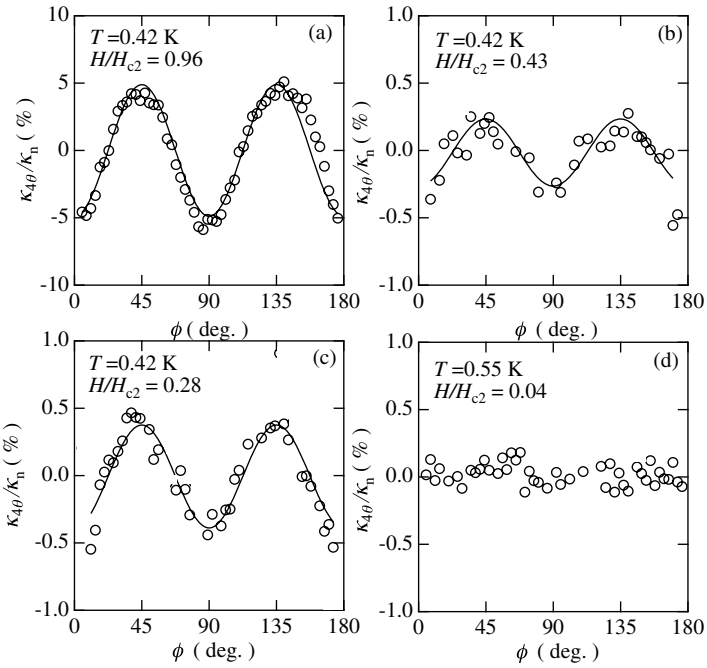

Figure 33. ((a)–(d)) The fourfold symmetry $\kappa_{4\phi}/\kappa_n$ at several fields obtained from figure 32(a).

estimated from the Abrikosov–Gorkov equation $\Psi(1/2 + \Gamma/2\pi T_c) - \Psi(1/2) = \ln(T_{c0}/T_c)$, where Ψ is a digamma function and T_{c0} is the transition temperature in the absence of the pair breaking. Assuming $T_{c0} = 1.50$ K and $\Delta = 1.76T_c$, Γ/Δ is estimated to be 0.025 (0.067) for

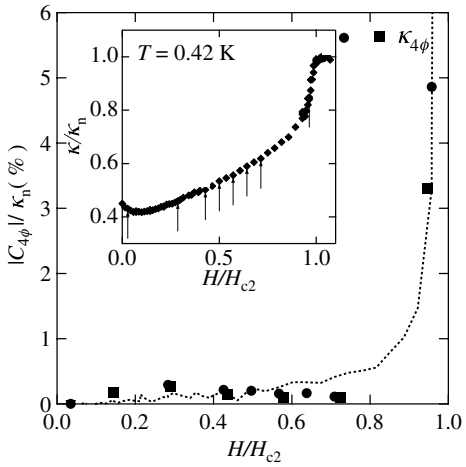

Figure 34. The amplitude of fourfold symmetry as a function of H/H_{c2}. The filled circles and squares indicate $|C_{4\theta}|/\kappa_n$ at $T = 0.42$ and 0.55 K, respectively. The solid line represents $|C_{4\theta}|/\kappa_n$ calculated from the fourfold symmetry of H_{c2}. Inset: H dependence of κ. The arrows indicates the points we measured $C_{4\theta}$.

$T_c = 1.45$ K ($T_c = 1.37$ K). Thus the dependence of κ(H) observed in very clean crystals is consistent with the κ of superconductors with line nodes.

We now discuss the angular variation of the thermal conductivity. Figures 32(a) and (b) depict $\kappa(\mathbf{H}, \phi)$ as a function of $\phi = (\mathbf{q}, \mathbf{H})$ [65]. In all the data κ(H, ϕ) can decomposed as in equation (15). Figures 33(a)–(d) show $\kappa_{4\phi}/\kappa_n$ as a function of ϕ after the subtraction of κ_0 and $\kappa_{2\phi}$ terms from κ. Figure 34 depicts the H dependence of $|C_{4\phi}|$. In the vicinity of H_{c2} where κ increases steeply, $|C_{4\phi}|/\kappa_n$ is of the order of a several per cent (see figure 33(a)). We point out that both the sign and amplitude of $C_{4\phi}$ in the vicinity of H_{c2} is mainly due to the in-plane anisotropy of H_{c2}. In figure 34, we plot the amplitude of the fourfold oscillation calculated from the in-plane anisotropy of H_{c2}. The calculation reproduces the data.

$|C_{4\phi}|/\kappa_n$ decreases rapidly and is about 0.2–0.3% at lower field where κ increases linearly with H (see figures 33(b) and (c)). At very low field where κ decreases with H, no discernible fourfold oscillation is observed within the resolution of $|C_{4\phi}|/\kappa_n < 0.1\%$ (see figure 33(d)). Thus the amplitude of the fourfold oscillation at low field of Sr_2RuO_4 is less than 1/20 of those in $CeCoIn_5$ and κ-$(ET)_2Cu(NCS)_2$. These results lead us conclude that the line nodes are not located perpendicular to the plane, but located parallel to the plane, i.e. horizontal node. If we accept the spin triplet superconductivity with broken time reversal symmetry, the gap symmetry which is most consistent with the in-plane variation of thermal conductivity is $\mathbf{d}(\mathbf{k}) = \Delta_0\hat{\mathbf{z}}(k_x + ik_y)(\cos ck_z + \alpha)$, in which the substantial portion of the Cooper pairs occurs between the neighbouring RuO_2 planes. Similar conclusion was obtained from the c axis thermal conductivity measurements [170]. Recently, the in-plane variation of heat capacity has been reported down to 100 mK. Below 200 mK, small but finite fourfold oscillation, which disappears at low H, was observed [72, 73]. This indicates that the gap function has a modulation around the c axis, though finite gap remains.

At an early stage, the gap symmetry of Sr_2RuO_4 was discussed in analogy with ^{3}He, where the Cooper pairs are formed by the exchange of ferromagnetic spin fluctuation [160]. However the inelastic neutron scattering experiments have shown the existence of strong incommensurate antiferromagnetic correlations and no sizable ferromagnetic spin fluctuations, indicating that the origin of the triplet pairing is not simply ferromagnetic [171]. The present

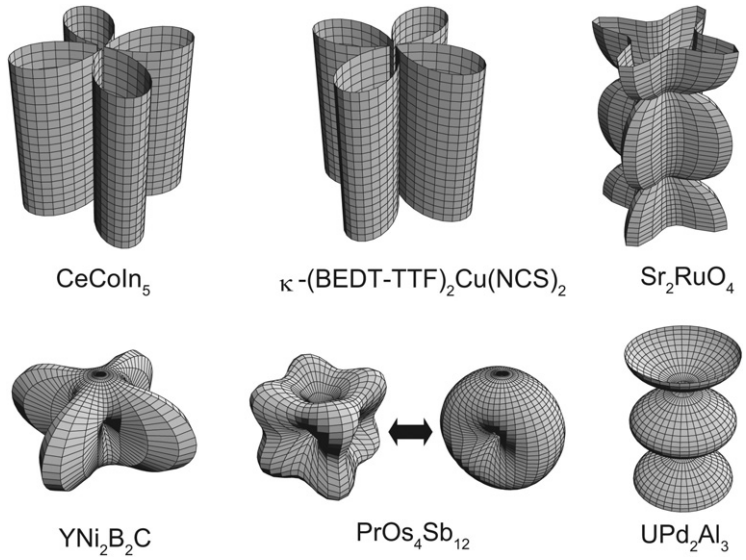

Figure 35. The nodal structure of several unconventional superconductors, including quasi-two dimensional heavy fermion $CeCoIn_5$, organic κ-$(BEDT\text{-}TTF)_2Cu(NCS)_2$, ruthenate Sr_2RuO_4 (the gap structure takes into account additional fourfold modulation as indicated by the specific heat measurements), borocarbide YNi_2B_2C, heavy fermion $PrOs_4Sb_{12}$, and heavy fermion UPd_2Al_3, which are determined by angular variation of the thermal conductivity.

results impose strong constraints on models that attempt to explain the mechanism of the triplet superconductivity. We finally comment on the orbital dependent superconductivity scenario, in which three different bands have different superconducting gaps [172]. In this case, our main conclusion can be applicable to the band with the largest gap (presumably the γ band).

8. Summary

In this paper, we discussed 'how do we determine the superconducting gap structure in the bulk?'. We show that the measurements of the thermal conductivity and specific heat in magnetic fields rotating in various directions relative to the crystal axis can determine the position and type of nodes. In figure 35, we summarize the nodal structure of several unconventional superconductors, including borocarbide YNi_2B_2C [67], heavy fermions UPd_2Al_3 [62], $CeCoIn_5$ [61], and $PrOs_4Sb_{12}$ [68], organic superconductor, κ-$(BEDT\text{-}TTF)_2Cu(NCS)_2$ [66], and ruthenate Sr_2RuO_4 [65], which are determined by the present technique. While more theoretical work is clearly needed to arrive at a more quantitative description of the data, we feel confident that the method provides a uniquely powerful route towards determination of the nodal structure in novel superconductors.

Acknowledgments

This work was done in collaboration with J Goryo, K Kamata, Y Kasahara, Y Nakajima, T Watanabe (University of Tokyo), P Thalmeier (Max-Planck Institute), and K Maki (University of Southern California). Samples were provided by Y Onuki, R Settai, H Shishido, Y Yoshida (Osaka University), Y Haga (Japan Atomic Research Institute), T Sasaki (Tohoku University), M Nohara, H Takagi (University of Tokyo), S Osaki, H Sugawara, H Sato (Tokyo Metropolitan University). We thank K Behnia, H Harima, P J Hirschfeld, M Ichioka, K Ishida,

H Kontani, K Kuroki, H Kusunose, J P Pascal, T Sakakibara, T Shibauchi, K Machida, V P Mineev, P Miranovic, Y Maeno, N Nakai, M Ogata, Y Tanaka, M Tanatar, M Udagawa, A Vorontsov, H Won, K Yamada and Y Yanase for valuable discussions. This work was partly supported by Grants-in-Aid for Scientific Research from MEXT (YM) and the Board of Regents of Louisiana (IV).

References

[1] Sigrist M and Ueda K 1991 *Rev. Mod. Phys.* **63** 239
[2] Mineev V P and Samokhin K V 1999 *Introduction to Unconventional Superconductivity* (London: Gordon and Breach)
[3] Steglich F, Aart F, Bredl C D, Lieke W, Meschede D, Franz W and Schafer H 1979 *Phys. Rev. Lett.* **43** 1892
[4] Stewart G R 1984 *Rev. Mod. Phys.* **56** 755
[5] Volovik G E and Gorkov L P 1985 *Zh. Eksp. Teor. Phys.* **88** 1412
Volovik G E and Gorkov L P 1985 *Sov. Phys.—JETP* **61** 843 (Engl. Transl.)
[6] Thalmeier P and Zwicknagl G 2005 *Handbook on the Physics and Chemistry of Rare Earths* vol 34 (Amsterdam: North-Holland)
[7] Tsuei C C and Kirtley J R 2000 *Rev. Mod. Phys.* **72** 969
[8] Maeno Y, Hashimoto H, Yoshida K, Nishizaki S, Fujita T, Bednorz J G and Lichtenberg F 1994 *Nature* **372** 532
[9] Bergemann C, Mackenzie A P, Julian S R, Forsythe D and Ohmichi E 2003 *Adv. Phys.* **52** 639
[10] Mackenzie A P and Maeno Y 2003 *Rev. Mod. Phys.* **75** 657
[11] Takada K, Sakurai H, Takayama-Muromachi E, Izumi F, Dilanian R A and Sasaki T 2003 *Nature* **422** 53
[12] Canfield P C, Gammel P L and Bishop L D 1998 *Phys. Today* **51** 40
[13] Jerome D, Mazaud A, Ribault M and Bechgaard K 1980 *J. Physique Lett.* **41** L95
[14] Kanoda K 1997 *Physica* C **282–287** 299
[15] McKenzie R H 1997 *Science* **278** 820
[16] Kuroki K 2006 *J. Phys. Soc. Japan* **75** 051013
[17] Kitaoka Y, Kawasaki S, Mito T and Kawasaki Y 2005 *J. Phys. Soc. Japan* **74** 186
[18] Tou H, Kitaoka Y, Asayama K, Kimura N, Onuki Y, Yamamoto E and Maezawa K 1996 *Phys. Rev. Lett.* **77** 1374
[19] Ishida K, Ozaki D, Kamatsuka T, Tou H, Kyogaku M, Kitaoka Y, Tateiwa N, Sato N K, Aso N, Geibel C and Steglich F 2002 *Phys. Rev. Lett.* **89** 037002
[20] Kohori Y, Matsuda K and Kohori T 1996 *J. Phys. Soc. Japan* **65** 1083
[21] Ott H R, Rudigier H, Rice T M, Ueda K, Fisk Z and Smith J L 1984 *Phys. Rev. Lett.* **52** 1915
[22] Tou H 2006 unpublished
[23] Lee I J, Brown S E, Clark W G, Strouse M J, Naughton M J, Kang W and Chaikin P M 2002 *Phys. Rev. Lett.* **88** 017004
[24] Ishida K, Mukuda H, Kitaoka Y, Asayama K, Mao Z Q, Mori Y and Maeno Y 1998 *Nature* **396** 658
[25] Fujiwara N, Mori N, Uwatoko Y, Matsumoto T, Motoyama N and Uchida S 2003 *Phys. Rev. Lett.* **90** 137001
[26] Mazin I I and Johannes M D 2005 *Nat. Phys.* **1** 91
[27] Kato M, Michioka C, Waki T, Itoh Y, Yoshimura K, Ishida K, Sakurai H, Takayama-Muromachi E, Takada K and Sasaki T 2006 *J. Phys.: Condens. Matter* **18** 669
[28] Saxena S S, Agarwal P, Ahilan K, Grosche F M, Haselwimmer R K W, Steiner M J, Pugh E, Walker I R, Julian S R, Monthoux P, Lonzarich G G, Huxley A, Sheikin I, Braithwaite D and Flouquet J 2000 *Nature* **406** 587
[29] Aoki D, Huxley A, Ressouche E, Braithwaite D, Flouquet J, Brison J P, Lhotel E and Paulsen C 2001 *Nature* **413** 613
[30] Akazawa T, Hidaka H, Fujiwara T, Kobayashi T C, Yamamoto E, Haga Y, Settai R and Onuki Y 2004 *J. Phys.: Condens. Matter* **16** L29
[31] Luke G M, Keren A, Le L P, Wu W D, Uemura Y J, Bonn D A, Taillefer L and Garrett J D 1993 *Phys. Rev. Lett.* **71** 1466
[32] Luke G M, Fudamoto Y, Kojima K M, Larkin M I, Merrin J, Nachumi B, Uemura Y J, Maeno Y, Mao Z Q, Mori Y, Nakamura H and Sigrist M 1998 *Nature* **394** 558
[33] Aoki Y, Tsuchiya A, Kanayama T, Saha S R, Sugawara H, Sato H, Higemoto W, Koda A, Ohishi K, Nishiyama K and Kadono R 2003 *Phys. Rev. Lett.* **91** 067003
[34] Izawa K, Kasahara Y, Matsuda Y, Behnia K, Yasuda T, Settai R and Onuki Y 2005 *Phys. Rev. Lett.* **94** 197002

[35] Yuan H Q, Agterberg D F, Hayashi N, Badica P, Vandervelde D, Togano K, Sigrist M and Salamon M B 2006 *Phys. Rev. Lett.* **97** 017006
[36] Borokowski L S and Hirschfeld P J 1994 *Phys. Rev.* B **49** 15404
[37] Volovik G E 1993 *JETP Lett.* **58** 469
[38] Tinkham M 2000 *Introduction to Superconductivity* (New York: Dover)
[39] Franz M and Tešanović Z 2000 *Phys. Rev. Lett.* **84** 554
[40] Knapp D, Kallin C and Berlinsky A J 2001 *Phys. Rev.* B **64** 014502
[41] Kübert C and Hirschfeld P J 1998 *Solid State Commun.* **105** 459
[42] Moler K A, Baar D J, Urbach J S, Liang R, Hardy W N and Kapitulnik A 1994 *Phys. Rev. Lett.* **73** 2744
[43] Moler K A, Sisson D L, Urbach J S, Beasley M R, Kapitulnik A, Baar D J, Liang R and Hardy W N 1997 *Phys. Rev.* B **55** 3954
[44] Vekhter I, Hirschfeld P J and Nicol E J 2001 *Phys. Rev.* B **64** 064513
[45] Kübert C and Hirshfeld P J 1998 *Phys. Rev. Lett.* **80** 4963
[46] Won H and Maki K 2000 *Physica* **341C–348C** 1647
[47] Durst A C, Vishwanath A and Lee P A 2003 *Phys. Rev. Lett.* **90** 187002
[48] Brandt U, Pesch W and Tewordt L 1967 *Z. Phys.* **201** 209
[49] Pesch W 1975 *Z. Phys.* B **21** 263
[50] Vekhter I and Houghton A 1999 *Phys. Rev. Lett.* **83** 4626
[51] Houghton A and Vekhter I 1998 *Phys. Rev.* B **57** 10831
[52] Kusunose H 2004 *Phys. Rev.* B **70** 054509
[53] Vorontsov A and Vekhter I 2006 *Phys. Rev. Lett.* **96** 237001
[54] Lowell J and Sousa J B 1970 *J. Low Temp. Phys.* **3** 65
[55] Kasahara Y, Shimono Y, Shibauchi T, Matsuda Y, Yonezawa S, Muraoka Y and Hiroi Z 2006 *Phys. Rev. Lett.* **96** 247004
[56] Barash Y S and Svidzinsky A A 1998 *Phys. Rev.* B **58** 6476
[57] Franz M 1999 *Phys. Rev. Lett.* **82** 1760
[58] Yu F, Salamon M B, Leggett A J, Lee W C and Ginsberg D M 1995 *Phys. Rev. Lett.* **74** 5136
[59] Aubin H, Behnia K, Ribault M, Gagnon R and Taillefer L 1997 *Phys. Rev. Lett.* **78** 2624
[60] Krishana K, Ong N P, Li Q, Gu G D and Koshizuka N 1997 *Science* **277** 83
[61] Izawa K, Yamaguchi H, Matsuda Y, Shishido H, Settai R and Onuki Y 2001 *Phys. Rev. Lett.* **87** 057002
[62] Watanabe T, Izawa K, Kasahara Y, Haga Y, Onuki Y, Thalmeier P, Maki K and Matsuda Y 2004 *Phys. Rev.* B **70** 184502
[63] Vekhter I, Hirschfeld P J, Carbotte J P and Nicol E J 1999 *Phys. Rev.* B **59** R9023
[64] Ocana R and Esquinazi P 2002 *Phys. Rev.* B **66** 064525
[65] Izawa K, Takahashi H, Yamaguchi H, Matsuda Y, Suzuki M, Sasaki T, Fukase T, Yoshida Y, Settai R and Onuki Y 2001 *Phys. Rev. Lett.* **86** 2653
[66] Izawa K, Yamaguchi H, Sasaki T and Matsuda Y 2002 *Phys. Rev. Lett.* **88** 027002
[67] Izawa K, Kamata K, Nakajima Y, Matsuda Y, Watanabe T, Nohara M, Takagi H, Thalmeier P and Maki K 2002 *Phys. Rev. Lett.* **89** 137006
[68] Izawa K, Nakajima Y, Goryo J, Matsuda Y, Osaki S, Sugawara H, Sato H, Thalmeier P and Maki K 2003 *Phys. Rev. Lett.* **90** 117001
[69] Aoki H, Sakakibara T, Shishido H, Settai R, Onuki Y, Miranovic P and Machida K 2004 *J. Phys.: Condens. Matter* **16** L13
[70] Park T, Salamon M B, Choi E M, Kim H J and Lee S I 2003 *Phys. Rev. Lett.* **90** 177001
[71] Park T, Chia E E M, Salamon M B, Bauer E D, Vekhter I, Thompson J D, Choi E M, Kim H J, Lee S I and Canfield P C 2004 *Phys. Rev. Lett.* **92** 237002
[72] Deguchi K, Mao Z Q and Maeno Y 2004 *J. Phys. Soc. Japan* **73** 1313
[73] Deguchi K, Mao Z Q, Yaguchi H and Maeno Y 2004 *Phys. Rev. Lett.* **92** 047002
[74] Hirschfeld P J 1998 *J. Korean Phys. Soc.* **33** 485
[75] Miranovic P, Nakai N, Ichioka M and Machida K 2003 *Phys. Rev.* B **68** 052501
[76] Nakai N, Miranovic P, Ichioka M and Machida K 2004 *Phys. Rev.* B **70** 100503
[77] Kusunose H 2004 *J. Phys. Soc. Japan* **73** 2512
[78] Won H K, Parker D, Haas S and Maki K 2004 *Curr. Appl. Phys.* **4** 523
[79] Udagawa M, Yanase Y and Ogata M 2004 *Phys. Rev.* B **70** 184515
[80] Udagawa M, Yanase Y and Ogata M 2005 *Phys. Rev.* B **71** 024511
[81] Kusunose H 2005 *J. Phys. Soc. Japan* **74** 1119
[82] Thalmeier P, Watanabe T, Izawa K and Matsuda Y 2005 *Phys. Rev.* B **72** 024539
[83] Adachi H, Miranovic P, Ichioka M and Machida K 2005 *Phys. Rev. Lett.* **94** 067007

[84] Maki K 1967 *Phys. Rev.* **158** 397
[85] Vekhter I and Hirschfeld P J 2000 *Physica* C **341–348** 1947
[86] Maki K, Thalmeier P and Won H 2002 *Phys. Rev.* B **65** 140502
[87] Thalmeier P and Maki K 2003 *Acta Phys. Pol.* B **34** 557
[88] Nohara M, Isshiki M, Sakai F and Takagi H 1999 *J. Phys. Soc. Japan* **68** 1078
[89] Izawa K, Shibata A, Matsuda Y, Kato Y, Takeya H, Hirata K, van der Beek C J and Konczykowski M 2001 *Phys. Rev. Lett.* **86** 1327
[90] Boaknin E, Hill R W, Proust C, Lupien C, Taillefer L and Canfield P C 2001 *Phys. Rev. Lett.* **87** 237001
[91] Yang I S, Klein M V, Cooper S L, Canfield P C, Cho B K and Lee S I 2000 *Phys. Rev.* B **62** 1291
[92] Yokoya T, Kiss T, Watanabe T, Shin S, Nohara M, Takagi H and Oguchi T 2000 *Phys. Rev. Lett.* **85** 4952
[93] Metlushko V, Welp U, Koshelev A, Aranson I, Crabtree G W and Canfield P C 1997 *Phys. Rev. Lett.* **79** 1738
[94] Nishimori H, Uchiyama K, Kaneko S, Tokura A, Takeya H, Hirata K and Nishida N 2004 *J. Phys. Soc. Japan* **73** 3247
[95] Kamata K 2002 *Master Thesis* University of Tokyo
[96] Kawano-Furukawa H, Takeshita H, Ochiai M, Nagata T, Yoshizawa H, Furukawa N, Takeya H and Kadowaki K 2002 *Phys. Rev.* B **65** 180508
[97] Kontani H 2004 *Phys. Rev.* B **70** 054507
[98] Eskildsen M R, Abrahamsen A B, Kogan V G, Gammel P L, Mortensen K, Andersen N H and Canfield P C 2001 *Phys. Rev. Lett.* **86** 5148
[99] Nakai N, Miranovic P, Ichioka M and Machida K 2002 *Phys. Rev. Lett.* **89** 237004
[100] Geibel C, Schank C, Thise S, Kitazawa H, Bredl C D, Bohm A, Rau M, Grauel A, Caspary R, Helfrich R, Ahlheim U, Weber G and Steglich F 1991 *Z. Phys.* B **84** 1
[101] Kita H, Donni A, Endoh Y, Kakurai K, Sato N and Komatsubara T 1994 *J. Phys. Soc. Japan* **63** 726
[102] Zwicknagl G, Yaresko A and Fulde P 2003 *Phys. Rev.* B **68** 052508
[103] Sato N K, Aso N, Miyake K, Shiina R, Thalmeier P, Varelogiannis G, Geibel C, Steglich F, Fulde P and Komatsubara T 2001 *Nature* **410** 340
[104] Jourdan M, Huth M and Adrian H 1999 *Nature* **398** 47
[105] Bernhoeft N 2000 *Eur. Phys. J.* B **13** 685
[106] Bernhoeft N, Hiess A, Metoki N, Lander G H and Roessli B 2004 *Preprint* cond-mat/0411042
[107] Metoki N, Haga Y, Koike Y and Onuki Y 1998 *Phys. Rev. Lett.* **80** 5417
[108] Abanov Ar and Chubukov A V 1999 *Phys. Rev. Lett.* **83** 1652
[109] Tou H, Kitaoka Y, Asayama K, Geibel C, Schank C and Stehlich F 1995 *J. Phys. Soc. Japan* **64** 725
[110] Chiao M, Lussier B, Ellman B and Taillefer L 1997 *Physica* B **230–232** 370
[111] Won H and Maki K 2002 *Vortices in Unconventional Superconductors and Superfluids* ed R P Huebener, N Schpohl and G E Volovik (Berlin: Springer)
[112] Tewordt L and Fay D 2005 *Phys. Rev.* B **72** 014502
[113] McHale P, Thalmeier P and Fulde P 2004 *Preprint* cond-mat/0401520
[114] Bauer E D, Frederick N A, Ho P C, Zapf V S and Maple M B 2002 *Phys. Rev.* B **65** 100506
[115] Aoki Y, Namiki T, Ohsaki S, Saha S R, Sugawara H and Sato H 2002 *J. Phys. Soc. Japan* **71** 2098
[116] Kotegawa H, Yogi M, Imamura Y, Kawasaki Y, Zheng G Q, Kitaoka Y, Ohsaki S, Sugawara H and Aoki Y 2003 *Phys. Rev. Lett.* **90** 027001
[117] Chia E E M, Salamon M B, Sugawara H and Sato H 2003 *Phys. Rev. Lett.* **91** 247003
[118] Seyfarth G, Brison J P, Measson M A, Flouquet J, Izawa K, Matsuda Y, Sugawara H and Sato H 2005 *Phys. Rev. Lett.* **95** 107004
[119] Joynt R and Taillefer L 2002 *Rev. Mod. Phys.* **74** 235
[120] Huxley A D, Measson M A, Izawa K, Dewhurst C D, Cubitt R, Grenier B, Sugawara H, Flouquet J, Matsuda Y and Sato H 2004 *Phys. Rev. Lett.* **93** 187005
[121] Cichorek T, Mota A C, Steglich F, Frederick N A, Yuhasz W M and Maple M B 2005 *Phys. Rev. Lett.* **94** 107002
[122] Pokrovskii V L 1961 *Sov. Phys.—JETP* **13** 447
[123] Petrovic C, Movshovich R, Jaime M, Pagliuso P G, Hundley M F, Sarrao J L, Fisk Z and Thompson J D 2001 *Eur. Phys. Lett.* **53** 354
[124] Sidorov V A, Nicklas M, Pagliuso P G, Sarrao J L, Bang Y, Balatsky A V and Thompson J D 2002 *Phys. Rev. Lett.* **89** 157004
[125] Curro N J, Simovic B, Hammel P C, Pagliuso P G, Sarrao J L, Thompson J D and Martins G B 2001 *Phys. Rev.* B **64** 180514
[126] Bianchi A, Movshovich R, Vekhter I, Pagliuso P G and Sarrao J L 2003 *Phys. Rev. Lett.* **91** 257001
[127] Nakajima Y, Izawa K, Matsuda Y, Uji S, Terashima T, Shishido H, Settai R, Onuki Y and Kontani H 2004 *J. Phys. Soc. Japan* **73** 5

[128] Movshovich R, Jaime M, Thompson J D, Petrovic C, Fisk Z, Pagliuso P G and Sarrao J L 2001 *Phys. Rev. Lett.* **86** 5152
[129] Kasahara Y, Nakajima Y, Izawa K, Matsuda Y, Behnia K, Shishido H, Settai R and Onuki Y 2005 *Phys. Rev.* B **72** 214515
[130] Kohori Y, Yamato Y, Iwamoto Y, Kohara T, Bauer E D, Maple M B and Sarrao J L 2001 *Phys. Rev.* B **64** 134526
[131] Ozcan S, Broun D M, Morgan B, Haselwimmer R K W, Waldram J R, Sarrao J L, Kamal S, Bidinosti C P and Turner P J 2003 *Europhys. Lett.* **62** 412
[132] Ormeno R J, Sibley A, Gough C E, Sebastian S and Fisher I R 2002 *Phys. Rev. Lett.* **88** 047005
[133] Chia E E M, Van Harlingen D J, Salamon M B, Yanoff B D, Bonalde I and Sarrao J L 2003 *Phys. Rev.* B **67** 014527
[134] Park W K, Greene L H, Sarrao J L and Thompson J D 2005 *Phys. Rev.* B **72** 052509
[135] Rourke P M C, Tanatar M A, Turel C S, Berdeklis J, Petrovic C and Wei J Y T 2005 *Phys. Rev. Lett.* **94** 107005
[136] Park W K, Greene L H, Sarrao J L and Thompson J D 2006 *Preprint* cond-mat/0606535
[137] Sheet G and Raychaudhuri P 2006 *Phys. Rev. Lett.* **96** 259701
Park W K and Greene L 2006 *Phys. Rev. Lett.* **96** 259702
[138] Tayama T, Harita A, Sakakibara T, Haga Y, Shishido H, Settai R and Onuki Y 2002 *Phys. Rev.* B **65** 180504
[139] Bianchi A, Movshovich R, Oeschler N, Gegenwart P, Steglich F, Thompson J D, Pagliuso P G and Sarrao J L 2002 *Phys. Rev. Lett.* **89** 137002
[140] Radovan H A, Fortune N A, Murphy T P, Hannahs S T, Palm E C, Tozer S W and Hall D 2003 *Nature* **425** 51
[141] Bianchi A, Movshovich R, Capan C, Pagliuso P G and Sarrao J L 2003 *Phys. Rev. Lett.* **91** 187004
[142] Watanabe T, Kasahara Y, Izawa K, Sakakibara T, Matsuda Y, van der Beek C J, Hanaguri T, Shishido H, Settai R and Onuki Y 2004 *Phys. Rev.* B **70** 020506
[143] Kakuyanagi K, Saitoh M, Kumagai K, Takashima S, Nohara M, Takagi H and Matsuda Y 2005 *Phys. Rev. Lett.* **94** 047602
[144] Tanatar M A, Paglione J, Nakatsuji S, Hawthorn D G, Boaknin E, Hill R W, Ronning F, Sutherland M, Taillefer L, Petrovic C, Canfield P C and Fisk Z 2005 *Phys. Rev. Lett.* **95** 067002
[145] Eskildsen M R, Dewhurst C D, Hoogenboom B W, Petrovic C and Canfield PC 2003 *Phys. Rev. Lett.* **90** 187001
[146] McKenzie R H 1997 *Science* **278** 820
[147] Schmalian J 1998 *Phys. Rev. Lett.* **81** 4232
[148] Mayaffre H, Wzietek P, Jerome D, Lenoir C and Batail P 1995 *Phys. Rev. Lett.* **75** 4122
[149] Desoto S M, Slichter C P, Kini A M, Wang H H, Geier U and Williams J M 1995 *Phys. Rev.* B **52** 10364
[150] Belin S, Behnia K and Deluzet A 1998 *Phys. Rev. Lett.* **81** 4728
[151] Carrington A, Bonalde I J, Prozorov R, Giannetta R W, Kini A M, Schlueter J, Wang H H, Geiser U and Williams J M 1999 *Phys. Rev. Lett.* **83** 4172
[152] Pinterić M, Tomić S, Prester M, Drobac D, Milat O, Maki K and Schweitzer D 2000 *Phys. Rev.* B **61** 7033
[153] Arai T, Ichimura K, Nomura K, Takasaki S, Yamada J, Nakatsuji S and Anzai H 2001 *Phys. Rev.* B **63** 104518
[154] Schrama J M, Rzepniewski E, Edwards R S, Singleton J, Ardavan A, Kurmoo M and Day P 1999 *Phys. Rev. Lett.* **83** 3041
[155] Elsinger H, Wosnitza J, Wanka S, Hagel J, Schweitzer D and Strunz W 2000 *Phys. Rev. Lett.* **84** 6098
[156] Vekhter I and Houghton A 2000 *Physica* C **341–348** 145
[157] Oshima K, Mori T, Inokuchi H, Urayama H, Yamochi H and Saito G 1988 *Phys. Rev.* B **38** 938
[158] Kuroki K, Kimura T, Arita R, Tanaka Y and Matsuda Y 2002 *Phys. Rev.* B **65** 100516
[159] Kondo H and Moriya T 2004 *J. Phys. Soc. Japan* **73** 812
[160] Rice T M and Sigrist M 1995 *J. Phys.: Condens. Matter* **7** L643
[161] Nelson K D, Mao Z Q, Maeno Y and Liu Y 2004 *Science* **306** 1151
[162] Zutic I and Mazin I 2005 *Phys. Rev. Lett.* **95** 217004
[163] NishiZaki S, Maeno Y and Mao Z Q 1999 *J. Low Temp. Phys.* **117** 1581
[164] Ishida K, Kitaoka Y, Asayama K, Ikeda S, Nishizaki S, Maeno Y, Yoshida K and Fujita T 1997 *Phys. Rev.* B **56** R505
[165] Suzuki M, Tanatar M A, Kikugawa N, Mao Z Q, Maeno Y and Ishiguro T 2002 *Phys. Rev. Lett.* **88** 227004
[166] Miyake K and Narikiyo O 1999 *Phys. Rev. Lett.* **83** 1423
[167] Hasegawa Y, Machida K and Ozaki M 2000 *J. Phys. Soc. Japan* **69** 336
[168] Graf M J and Balatsky A V 2000 *Phys. Rev.* B **62** 9697
[169] Kuwabara T and Ogata M 2000 *Phys. Rev. Lett.* **85** 4586
[170] Tanatar M A, Suzuki M, Nagai S, Mao Z Q, Maeno Y and Ishiguro T 2001 *Phys. Rev. Lett.* **86** 2649
[171] Sidis Y, Braden H, Bourges P, Hennion B, NishiZaki S, Maeno Y and Mori Y 1999 *Phys. Rev. Lett.* **83** 3320
[172] Agterberg D F, Rice T M and Sigrist M 1997 *Phys. Rev. Lett.* **78** 3374

[173] Takigawa M, Yasuoka H and Saito G 1987 *J. Phys. Soc. Japan* **56** 873
[174] Fujimoto T, Zheng G Q, Kitaoka Y, Meng R L, Cmaidalka J and Chu C W 2004 *Phys. Rev. Lett.* **92** 047004
[175] Kobayashi Y, Watanabe H, Yokoi M, Moyoshi T, Mori Y, Sato M, Yokoi M and Sato M 2005 *J. Phys. Soc. Japan* **74** 1800
[176] Zheng G Q, Matano K, Chen D P and Lin C T 2006 *Phys. Rev.* B **73** 180503
[177] Maki K, Thalmeier P and Won H 2002 *Phys. Rev.* B **65** 140502
[178] Ueda K, Kitaoka Y, Yamada H, Kohori Y, Kohara T and Asayama K 1987 *J. Phys. Soc. Japan* **56** 867
[179] Kawasaki S, Mito T, Kawasaki Y, Zheng G Q, Kitaoka Y, Shishido H, Araki S, Settai R and Onuki Y 2002 *Phys. Rev.* B **66** 054521
[180] Kohori Y, Yamato Y, Iwamoto Y and Kohara T 2000 *Eur. Phys. J.* B **18** 601
[181] Belin S and Behnia K 1997 *Phys. Rev. Lett.* **79** 2125
[182] Bauer E, Hilscher G, Michor H, Paul C, Scheidt E W, Gribanov A, Seropegin Y, Noel H, Sigrist M and Rogl P 2004 *Phys. Rev. Lett.* **92** 027003
[183] Yuan H Q, Grosche F M, Deppe M, Geibel C, Sparn G and Steglich F 2003 *Science* **302** 2104
[184] Matsuda K, Kohori Y and Kohori T 1996 *J. Phys. Soc. Japan* **65** 679
[185] Joynt R and Taillefer L 2002 *Rev. Mod. Phys.* **74** 235
[186] Kotegawa H, Harada A, Kawasaki S, Kawasaki Y, Kitaoka Y, Haga Y, Yamamoto E, Onuki Y, Itoh K M, Haller E E and Harima H 2005 *J. Phys. Soc. Japan* **74** 705
[187] Curro N J, Caldwell T, Bauer E D, Morales L A, Graf M J, Bang Y, Balatsky A V, Thompson J D and Sarrao J L 2005 *Nature* **434** 622
[188] Sakai H, Tokunaga Y, Fujimoto T, Kambe S, Walstedt R E, Yasuoka H, Aoki D, Homma Y, Yamamoto E, Nakamura A, Shiokawa Y, Nakajima K, Arai Y, Matsuda T D, Haga Y and Onuki Y 2005 *J. Phys. Soc. Japan* **74** 1710
[189] Maclaughlin D E, Tien C, Clark W G, Lan M D, Fisk Z, Smith J L and Ott H R 1984 *Phys. Rev. Lett.* **53** 1833